JOURNAL OF GEOPHYSICAL RESEARCH, VOL. 106, NO. D2, PAGES 1551–1568, JANUARY 27, 2001

Global direct radiative forcing due to multicomponent anthropogenic and natural aerosols

Mark Z. Jacobson

Department of Civil and Environmental Engineering, Stanford University, Stanford, California

Abstract. Global simulations of the composition of and direct forcing due to aerosols containing natural and/or anthropogenic sulfate, nitrate, chloride, carbonate, ammonium, sodium, calcium, magnesium, potassium, black carbon, organic matter, silica, ferrous oxide, and aluminum oxide were carried out. Chloride and natural sulfate were found to be the most important natural aerosol constituents in the atmosphere in terms of solar plus thermal-infrared forcing. Sea spray was the most important natural aerosol type, indicating that it should be accounted for in weather and climate calculations. Ammonium was found to have a positive direct forcing, since it reduces water uptake in sulfate-containing solutions; thus, anthropogenic ammonium contributes to global warming. The magnitudes of ammonium and nitrate forcing were smaller than those of chloride or sulfate forcing. When organics were divided into three groups with different assumed UV absorption characteristics, total aerosol direct forcing at the tropopause increased by about +0.03 to +0.05 W m^{-2} (direct forcing by organics remained negative), suggesting that UV absorption by organics is a nontrivial component of the global energy balance. Gypsum [$CaSO_4$-$2H_2O$], sal ammoniac [NH_4Cl], halite [NaCl], halite, and nitrum [KNO_3] were estimated to be the most common sulfate-, ammonium-, sodium-, chloride-, and nitrate-containing solid-phase aerosol constituents, respectively, in the global atmosphere. Solid formation in aerosols was found to increase total-aerosol direct forcing by +0.03 to +0.05 W m^{-2}. Spatial and vertical forcing estimates, sensitivities of forcing to relative humidity and concentration, and estimates of global aerosol liquid water content are given. Modeled aerosol optical properties are compared with satellite and field measurements.

1. Introduction

To date, many global studies of direct forcing due to anthropogenic sulfate, black (elemental) carbon (BC), soil dust, and organic matter (OM) have been carried out [e.g., *Charlson et al.*, 1991; *Kiehl and Briegleb*, 1993; *Taylor and Penner*, 1994; *Boucher and Anderson*, 1995; *Tegen et al.*, 1996; *Chuang et al.*, 1997; *Feichter et al.*, 1997; *Hansen et al.*, 1997; *Stenchikov et al.*, 1998; *Haywood and Ramaswamy*, 1998; *Myhre et al.*, 1998; *Penner et al.*, 1998; *Miller and Tegen*, 1998; *Hansen et al.*, 1998; *Jacobson*, 2000]. This is a global study of the direct solar plus thermal-IR forcing due to natural and anthropogenic sulfate, nitrate, chloride, carbonate, ammonium, sodium, calcium, magnesium, potassium, BC, OM, silica, ferrous oxide, aluminum oxide, and other components.

A goal of the study is to examine the solar plus thermal-IR direct forcing due to size-resolved sea-spray drops and their individual components. Previously, *Tegen et al.* [1997] estimated the sea-spray aerosol extinction optical depth at 550 nm with a global transport model. *Quinn and Coffman* [1999] and others calculated the extinction optical depth at individual locations. *Jacobson* [1998, 1999a] found that sea spray constituents and sea-spray drops as a whole were among the most important aerosol constituents in the atmosphere in terms of global direct forcing under clear-sky and all-sky (clear plus cloudy sky) conditions. Subsequently, *Haywood et al.* [1999] discussed the direct, clear-sky solar forcing, over the oceans, of bulk sea-spray drops relative to other aerosol types. This paper expands on the study work of *Jacobson* [1998; 1999a] to examine the importance of sea spray and its individual components. This study also examines global-scale aerosol composition and liquid water content (LWC), natural and anthropogenic aerosol forcing estimates when BC is treated as a core for particle optics, the effect of ultraviolet (UV) absorption by particulate OM on forcing, and the effect of solid formation on forcing.

Paper number 2000JD900514.
0148-0227/01/2000JD900514$09.00

2. Model Description

2.1. Dynamics

The global model used here is GATORG (Gas, Aerosol, Transport, Radiation, and General circulation model), which was derived from the limited-area model GATORM [*Jacobson* 1999b] by replacing the dynamics code in GATORM with a 1994 version of the University of California at Los Angeles General Circulation Model [*Arakawa and Lamb*, 1981], replacing heating rates in the GCM with those from GATORM's radiation code, and replacing the original Arakawa-Schubert (A-S) cumulus parameterization with a modified A-S parameterization [*Ding and Randall*, 1998]. The gas-aerosol-radiative portions of GATORG are the same as those in GATORM.

The model's resolution was set to 4° S-N x 5° W-E with 22 sigma-pressure layers from the ground to the top-of-the-atmosphere (TOA) of 0.425 mbar (≈55 km). Initial

Table 1. List of Aerosol Components Carried in Each Size Bin in the Model and Information About How Their Concentrations were Determined and Whether Refractive Index (RI) Data Were Available for Them[a]

Species	Concentration Source	Initial Burden, Tg	RI Data?
H_2O(aq)	CM, EQ	--	Yes
H_2CO_3(aq)	EQ	--	RP
H_2SO_4(aq)	EQ	--	Yes
H+	EQ	--	PM
NH_4^+	T2, EQ	BD	PM
Na^+	T2, EQ.	0.96	PM
Mg^{2+}	T2, EQ	0.14	PM
Ca^{2+}	T2, EQ	0.16	PM
K^+	T2, EQ	0.05	PM
HSO_4^-	EQ	--	PM
SO_4^{2-}	SR, T2,EQ	BD	PM
NO_3^-	T2, EQ	0.38	PM
Cl^-	T2, EQ	1.79	PM
Br-	T2	.002	PM
HCO_3^-	EQ	--	PM
CO_3^{2-}	EQ	--	PM
NH_4NO_3(s)	EQ	--	Yes
NH_4Cl(s)	EQ	--	Yes
NH_4HSO_4(s)	EQ	--	Yes
$(NH_4)_2SO_4$(s)	EQ	--	Yes
$(NH_4)_3H(SO_4)_2$(s)	EQ	--	Yes
$(NH_4)_2CO_3$(s)	EQ	--	RP
NaNO3(s)	EQ	--	Yes
NaCl(s)	EQ	--	Yes
NaHSO4(s)	EQ	--	Yes
Na_2SO_4(s)	EQ	--	Yes
Na_2CO_3(s)	SP, EQ	0.39	Yes
KNO_3(s)	EQ	--	Yes
KCl(s)	EQ	--	Yes
$KHSO_4$(s)	EQ	--	Yes
K_2SO_4(s)	EQ	--	Yes
K_2CO_3(s)	SP, EQ	0.45	Yes
$Ca(NO3)_2$(s)	EQ	--	RP
$CaCl_2$(s)	EQ	--	Yes
$CaSO_4$(s)	EQ	--	Yes
$CaCO_3$(s)	SP, EQ	1.08	Yes
$Mg(NO_3)_2$(s)	EQ	--	RP
$MgCl_2$(s)	EQ	--	Yes
MgSO4(s)	EQ	--	Yes
$MgCO_3$(s)	SP, EQ	0.83	Yes
SiO_2(s)	SP	9.18	Yes
Al_2O_3(s)	SP	2.16	Yes
Fe_2O_3(s)	SP	1.05	Yes
BC	ER	0.23	Yes
OM1	OR	0.51	Yes
OM2	OR	0.36	Yes
OM3	OR	0.09	Yes

[a] Also shown are initial globally and annually averaged aerosol burdens of the 20 key aerosol constituents, before equilibrium calculations. Burdens are natural plus anthropogenic burdens in all cases. Where no initial burden occurs, the species concentration was not initialized, but was subsequently calculated with the equilibrium solver. The total dry soil dust burden was 15.1 Tg, calculated by summing the burdens due to SiO_2, Al_2O_3, $Fe2O_3$, Na_2CO_3, K_2CO_3, $MgCO_3$, and $CaCO_3$. The total dry sea spray aerosol burden was approximately 3.3 Tg, calculated by summing the burdens of Na^+, Mg^{2+}, Ca^{2+}, K^+, Cl^-, Br^-, and 25% of Na^+ for $ssSO_4^{2-}$. Concentration sources are as follows: CM, from cloud module calculations in GATORG; EQ, from equilibrium calculation in GATORG; T2, from Table 2b; SR, global near-surface and 600 mbar anthropogenic S(VI) concentrations were obtained from Langner and Rodhe [1991]. Anthropogenic S(VI) was assumed to exist in nucleation- and accumulation-mode particles, since this data set did not include sources for coarse-mode particles. Thus, information from only the first two columns in Table 2c were used to distribute anthropogenic S(VI). Natural S(VI) concentrations were obtained from Table 2b and from SAGE II data, as described in the text; SP, the initial concentrations of soil dust components were partitioned from global near-surface and zonally averaged 600 mbar model predictions from Dentener et al. [1996] with the partitioning fractions listed in Section 2.3 here. The masses for each component were further partitioned into accumulation and coarse-particle modes for each region with mass fractions given in Tables 2b and 2c; ER, the initial concentrations of BC were obtained by partitioning the near-surface January and July and zonally averaged upper tropospheric model predictions of BC from Cooke and Wilson [1996] into nucleation, accumulation, and coarse modes with the mass fractions given in Table 2c. The lognormal parameters used for each mode are given in Table 2a. Concentrations were reduced by 15% in the baseline simulation, as described in the text.; OR, the initial concentrations of OM were obtained by partitioning the near-surface January and July and zonally averaged upper tropospheric model predictions of OM from Liousse et al. [1996] into nucleation, accumulation, and coarse modes with the mass fractions given in Table 2c. The lognormal parameters used for each mode are given in Table 2a. The total OM in each mode was further divided into three types of OM (OM1, OM2, OM3), each with different optical characteristics, as described in the text.; PM, indicates that the ions were combined into hypothetical aqueous electrolytes, and partial molar refractions of the electrolytes were used in refractive index calculations; RP, indicates that refractive index data were not available, and the partial molar refractions of the corresponding aqueous electrolyte was used to calculate the solid's refractive indices; BD, tropospheric (below the Junge layer-- see Figure 2a) burdens of NH_4^+ and SO_4^{2-} were 0.41 and 2.23 Tg, respectively. Junge-layer burdens were 0.31 and 2.31 Tg, respectively.

temperature, water vapor, and wind fields were obtained from an October 1, 1998 3-D global climatological database. Sea-surface temperatures were calculated in time assuming a fixed ocean mixed-layer depth. Surface albedos were interpolated each day from a monthly averaged global data set [NASA Data System Staff, 1992], except that snow and sea ice albedos were calculated according to changes in modeled snow cover and sea-ice cover, respectively. The model was first integrated in time for one year to generate 3-D fields of temperature, water vapor, and relative humidity (RH), and cloud liquid and ice water contents. These fields were written to files on six days -- the 15th of January, March, May, July, September, and November, each at 0:00, 06:00, 12:00, and 18:00 Greenwich Mean Time (GMT) (24 files were written). The model was then rerun for each of the 24 cases in equilibrium mode to calculate aerosol composition and radiative fields. Although accuracy improves with greater time resolution, an increase from 4 to 24 simulations changed total-aerosol forcing predictions by <15%, and test cases of an increase from 24 to 72 simulations (6 days, 12 hours per day) changed forcing predictions by <6%.

2.2. Thermodynamics

The model treated 47 aerosol species, identified in Table 1, in each of 17 size bins. Of the 47 species, concentrations of 39 (identified with an EQ in Table 1) were determined from equilibrium calculations. Of these 39, 12 (those identified with an EQ and that have an initial burden in Table 1) were initialized with trimodal distributions over 17 size bins. Equilibrium equations were solved in each bin with EQUISOLV II [*Jacobson*, 1999c] among the 39 constituents to distribute initial burdens among ions and solids and to calculate aerosol LWC. EQUISOLV II iterates temperature-dependent equilibrium, solute activity-coefficient, and water activity-

coefficient equations. The code is mass and charge conserving and unconditionally stable. Aside from equilibrium uptake of liquid water due to hydration, no gas-aerosol transfer calculations were performed; thus, all initialized material was retained in each bin.

The remaining eight (out of 47) species in Table 1 were initialized with trimodal distributions, and their concentrations were internally mixed with those of the 39 other constituents in each bin (except that BC was treated as a core for baseline optical calculations). No physical or chemical processes affected these eight species.

Predicted RHs affect aerosol composition in two ways in the model. First, at high RHs, dissolved electrolytes hydrate more liquid water than at low RHs, increasing aerosol LWC, increasing particle size, and decreasing solute molality. Dissolved electrolytes in the model that affect water uptake include molecular $H_2SO_4(aq)$ and all combinations of cation/anion pairs in Table 1 [e.g., H^+/HSO_4^-, $2H^+/SO_4^{2-}$, Na^+/Cl^-, $2Na^+/SO_4^{2-}$,..., etc.]. Since sea spray, soil dust, and sulfate all contain soluble electrolytes, variations in RH affect sea spray, soil dust, and sulfate forcing through changes in LWC. For this study, OM was assumed to be nonhygroscopic due to the dearth of information about the composition and water uptake of OM. Aerosols can contain hundreds of OM compounds, 20-67% of which are water soluble [*Saxena and Hildemann*, 1996]. The ability of soluble organics to hydrate varies by compound, making an estimate of water uptake difficult at this time.

Second, solid electrolyte formation is sensitive to RH. When the RH is increasing and rises above the deliquescence RH (DRH) of a solid, the solid, if present, must dissociate. When the RH is decreasing, dissolved electrolytes cannot precipitate until their crystallization RH (CRH) is reached. For the baseline simulation (DRH case), a solid was permitted to exist when the RH was less than the solid's DRH (although whether the solid actually existed depended on whether electrolytes were supersaturated in solution). A sensitivity test was run (CRH case) to examine the effect of this assumption versus a metastable-state assumption, where a solid was not permitted to exist until the RH dropped below the solid's CRH. Total aerosol direct forcing at the tropopause in the CRH case was 0.03 W m^{-2} more negative than in the DRH case. In a second test, where no solids at all were allowed to form, the forcing was 0.05 W m^{-2} more negative than in the DRH case. The effect of solid formation was small for two reasons: (1) The most important size regime for radiative forcing is the accumulation mode, but solids forming in this mode, particularly ammonium bisulfate [NH_4HSO_4] and mascagnite [$(NH_4)_2SO_4$], have DRHs of 40 and 80%, respectively; thus, when these solids precipitate from solution, the RH is usually low, and the corresponding loss of liquid water is relatively small; (2) most aerosols on Earth are in the boundary layer over the oceans, where the RH is generally high and solid formation is somewhat inhibited.

Once initial equilibrium aerosol compositions were calculated, solution densities in each size bin were obtained by combining ions into electrolytes and using the method described by *Tang* [1997]. Solution densities were combined with solid densities and wet-mass concentrations from EQUISOLV II to estimate wet-volume concentrations of total material in each bin. Wet-volume concentrations were divided by single-particle volumes to estimate number concentrations, required for optical calculations.

Table 2a. Geometric Mean Volume Radii (r_n, r_a, r_c) and Geometric Standard Deviations (σ_n, σ_a, σ_c) for Nucleation, Accumulation, and Coarse-Particle Modes, Respectively, for Each of Five Regions of the Atmosphere

	r_n, μm	r_a, μm	r_c, μm	σ_n	σ_a	σ_c
Continental	0.015[b]	0.175[b]	3.0[b]	1.6[b]	2.1[b]	2.2[b]
NH Ocean	0.01[c]	0.24[d]	2.96[d]	1.6[b]	2.0[e]	2.1[d]
SH Ocean	0.01[c]	0.24[d]	2.96[d]	1.6[e]	2.0[e]	2.1[d]
Polar	0.01[e]	0.24[e]	2.96[e]	1.6[e]	2.0[e]	2.1[e]
Upper trop.	0.01[e]	0.24[e]	1.1[f]	1.6[e]	2.0[e]	2.0[f]

[a]NH is the Northern Hemisphere, SH is the Southern Hemisphere. The only variations to these values were that r_n was 0.045 and 0.054 μm for BC and OM, respectively [*Venkataraman et al.*, 1994], r_c and σ_c were 1.0 μm and 1.85, respectively, for BC [*Berner et al.*, 1996], and r_c and σ_c were 1.25 μm and 1.85, respectively, for OM [assumed the same as ambient aerosol from *Berner et al.*, 1996].

[b]*Whitby* [1978], Clean-continental parameters.

[c]*Whitby* [1978], Nucleation-mode parameters for marine environment.

[d]*Krekov* [1993, Table 1.6, mean accumulation- and coarse-mode parameters].

[e]Estimated from ocean values.

[f]*Krekov* [1993, Table 1.9, parameters for g2 distribution at 5 km].

2.3. Initial Aerosol Fields

Initial aerosol fields were obtained from several sources. Trimodal lognormal distribution information for some key constituents (Na^+, K^+, Ca^{2+}, Mg^{2+}, natural S(VI), NO_3^-, Cl^-, and Br^-) are given in Tables 2a, 2b, and 3 for several atmospheric regions. In the case of other key constituents, global surface and either elevated or zonally averaged latitude-altitude concentration distributions were digitized from model-study maps. Anthropogenic S(VI) distributions were obtained from *Langner and Rodhe* [1991, Figures 5b and 6b], total BC distributions were obtained from Cooke and Wilson [1996, Figures 5a, 5b, 11a, and 11b], total OM distributions were obtained from Liousse et al. [1996, Figures 4a, 4b, and 13a], and total soil dust distributions were obtained from Dentener et al. [1996, Figures 4a and 4c]. BC and OM maps, available for January and July, were interpolated in time. Maps for sulfate and soil dust were annual average maps, and the same map, in both cases, was used every month. Total concentrations from the digitized maps were partitioned into trimodal lognormal distributions with the mass fraction information given in Table 2c, as described in the footnotes for Table 1. Whereas the use of an annual average map for sulfate leads to errors, the globally integrated error is not expected to be large, since the seasonal variation in anthropogenic SO_2 emissions is only about +/-11% of the annual average [E. C. Voldner et al., 1°x1° global SO_x and NO_x 2-level inventory resolved seasonally into emission sectors and point and area emissions sources, Global Emissions Inventory Activity (GEIA) web site, www.onesky.umich.edu/geia/, 1999]. Even though an annual dry-mass map was used for sulfate and soil dust, their forcings varied each of the 24 simulations, since forcings depend on particle composition and size, which vary with predicted RH and temperature in the model.

Cooke et al. [1999] revised the fossil-fuel-portion of the inventory of *Cooke and Wilson* [1996] and estimated a new fossil fuel plus biomass burning BC burden of 0.15-0.25 Tg

Table 2b. Estimated Nucleation, Accumulation, and Coarse-Mode Masses for Each of Five Regions

	M_n, ng m^{-3}	M_a, ng m^{-3}	M_c, ng m^{-3}
	Na^+		
Continental	0.01[a]	2.5[b]	48[b]
NH Oceans	0.6[a]	120[c]	2410[c]
SH Ocean	0.9[a]	170[c]	2440[c]
Polar	0.06[a]	12[d]	210[d]
Midtroposphere	0.005[a]	1[e]	19[e]
	K^+		
Continental	0.02[a]	6[b]	64[b]
NH Oceans	0.08[a]	15.7[c]	134[c]
SH Ocean	0.05[a]	10[c]	115[c]
Polar	0.03[a]	6[f]	62[f]
Midtroposphere	0.004[a]	0.7[g]	7.3[g]
	Ca^{2+}		
Continental	0.07[a]	17[b]	153[b]
NH Oceans	0.3[a]	54.5[c]	485[c]
SH Ocean	0.1[a]	25.9[c]	238[c]
Polar	0.1[a]	20.1[f]	181[f]
Midtroposphere	0.01[a]	2[e]	1.8[e]
	Mg^{2+}		
Continental	0.03[a]	7[h]	78[h]
NH Oceans	0.2[a]	33.4[c]	331[c]
SH Ocean	0.2[a]	32.8[c]	399[c]
Polar	0.09[a]	17[f]	180[f]
Midtroposphere	0.003[a]	0.5[e]	5.5[e]
	Natural S(VI)		
Continental	0.07[a]	18[f]	450[i]
NH Oceans	0.2[a]	31[c]	610[c]
SH Ocean	0.2[a]	42[c]	620[c]
Polar	0.09[a]	18[f]	310[f]
Midtroposphere	0.2[a]	40[g]	120[g]
	NO_3^-		
Continental	0.2[a]	60[b]	840[b]
NH Oceans	0.05[a]	10.5[c]	182[c]
SH Ocean	0.05[a]	9.1[c]	92[c]
Polar	0.03[a]	4.9[f]	69[f]
Midtroposphere	0.03[a]	6.7[g]	93[g]
	Cl^-		
Continental	0.02[a]	4[b]	110[b]
NH Oceans	0.7[a]	138[c]	4920[c]
SH Ocean	1[a]	259[c]	4270[c]
Polar	0.08[a]	15[d]	350[d]
Midtroposphere	0.003[a]	0.6[g]	15[g]
	Br^-		
Continental	0.07[a]	18[j]	5[j]
NH Oceans	0.003[a]	0.58[c]	3.02[c]
SH Ocean	0.0006[a]	0.12[c]	5.95[c]
Polar	0.003[a]	0.59[d]	7.6[d]
Midtroposphere	0.001[a]	0.2[g]	2.9[g]

[a]Nucleation-mode concentrations for continents were scaled with the nucleation: accumulation mode volume concentration ratio from the continental distribution of *Whitby* [1978]. Those for ocean, polar, and upper tropospheric environments were scaled with the nucleation:accumulation mode volume concentration ratio for marine environments from the same source.

[b]*Pueschel* [1995, Table 5.2]. The average continental value was partitioned between the accumulation and coarse modes with the average ocean accumulation:coarse mode concentration ratio for the same species, given here.

[c]Data compiled by *Quinn et al.* [1998], extracted by A. Fridlind.

[d]*Sturges and Barrie* [1988]. Partitioned here between the accumulation and coarse modes with the average ocean accumulation:coarse mode concentration ratio for the same species, given here..

[p. 22,149]. To conform with the revised estimate, the BC distributions extracted from *Cooke and Wilson* [1996] were reduced by 15% so that the baseline yearly-averaged total burden of BC from fossil fuels and biomass burning in this study was 0.23 Tg, within the range of the revised estimate. Whereas, *Bond et al.* [1998] further suggest that non-residential coal-burning-BC emission factors of *Cooke and Wilson* [1996] may have been overestimated, Bond et al. also state that their results were preliminary and may not be representative of all coal-burning plants. Due to the uncertainty, the BC inventory was not adjusted further here.

Initial soil dust mass in each grid cell in the model was partitioned with soil dust composition data from *Gillette et al.*, [1993, Table 2.3] in the following manner: 60.0% SiO_2(s), 14.1% Al_2O_3(s), 6.85% Fe_2O_3(s), 7.04% $CaCO_3$(s), 5.45% $MgCO_3$(s), 2.95% K_2CO_3(s), and 2.55% Na_2CO_3(s). Soil dust was internally mixed with other particle components. Since soil-dust electrolytes interacted with non-soil-dust electrolytes during equilibrium calculations, the composition and LWC of particles containing soil dust varied during simulations.

Stratospheric sulfate size distributions were extracted from 1992 Stratospheric Aerosol and Gas Experiment (SAGE II) surface-area data [*Thomason et al.*, 1997], lognormal parameter/sulfate weight-percent estimates versus altitude [*Krekov*, 1993, Tables 1.9 and 1.15], and aerosol number concentration data versus altitude [*Deshler et al.*, 1992].

Initial near-surface mass concentrations for each key species were distributed with trimodal lognormal distributions over 17 model size bins, geometrically spaced from 0.01-53 μm in radius. Near-surface concentrations were assumed to be well-mixed in the air mass up to 150 m over the ocean in summer and winter, up to 300 m over continents in summer, and up to 500 m over continents in winter [*Krekov*, 1993, Table 1.3]. The mixing heights for spring and autumn were averaged between those of winter and summer over both oceans and continents. Upper-tropospheric aerosol masses were estimated primarily from the data of *Talbot et al.* [1998], *Tabazadeh et al.* [1998], and *Li et al.* [1997], as described in Table 2b. Values for S(VI), total BC, total OM, and total soil dust aloft were obtained from *Langner and Rodhe* [1991], *Cooke and Wilson* [1996], *Liousse et al.* [1996], and *Dentener et al.* [1996], respectively. These values were also distributed over 17 model

[c]*Li et al.* [1997] for 5.5 km. Total mass data were partitioned here between the accumulation and coarse modes with the average ocean accumulation:coarse mode concentration ratio for the same species, given here.

[f]Estimated as 50% of average ocean values.

[g]Average data gathered by *Talbot et al.* [1998] for 5.5 km, shown in *Tabazadeh et al.* [1998, Figure 2]. Total mass data were partitioned here between the accumulation and coarse modes with the average ocean accumulation:coarse mode concentration ratio for the same species, given here. For natural S(VI), the resulting upper-tropospheric accumulation-mode mass was multiplied by 0.3 to estimate the natural portion of S(VI).

[h]Estimated as 50% of total continental Ca^{2+}, distributed between the accumulation and coarse modes with the average Mg^{2+} ocean accumulation:coarse mode concentration ratio, given here.

[i]*Pueschel* [1995, Table 5.2]. The average continental value was partitioned here between the accumulation and coarse modes with the average ocean accumulation:coarse mode concentration ratio for non-sea-salt sulfate, shown in Table 3.

[j]*Finlayson-Pitts and Pitts* [1986, Table 12.14].

Table 2c. Estimated Nucleation-, Accumulation-, and Coarse-Mode Mass Fractions for Each of Five Regions

	f_n	f_a	f_c
	BC		
Continental	0..093[a]	0.578[a]	0.329[a]
NH Oceans	0..093[a]	0.578[a]	0.329[a]
SH Ocean	0..093[a]	0.578[a]	0.329[a]
Polar	0..093[a]	0.578[a]	0.329[a]
Midtroposphere	0..093[a]	0.578[a]	0.329[a]
	Anthropogenic S(VI)		
Continental	0.003[b]	0.834[c]	0.163[c]
NH Oceans	0.004[b]	0.846[d]	0.150[d]
SH Ocean	0.004[b]	0.805[d]	0.191[d]
Polar	0.003[b]	0.510[e]	0.487[e]
Midtroposphere	0.003[b]	0.510[e]	0.487[e]
	$Al_2O_3(s)$		
Continental	0	0.217[f]	0.783[f]
NH Oceans	0	0.217[f]	0.783[f]
SH Ocean	0	0.217[f]	0.783[f]
Polar	0	0.217[f]	0.783[f]
Midtroposphere	0	0.217[f]	0.783[f]
	OM		
Continental	0.004[b]	0.876[c]	0.120[c]
NH Oceans	0.004[b]	0.689[g]	0.307[g]
SH Ocean	0.004[b]	0.689[g]	0.307[g]
Polar	0.002[b]	0.678[e]	0.320[e]
Midtroposphere	0.002[b]	0.678[e]	0.320[e]
	$SiO_2(s)$		
Continental	0	0.143[f]	0.857[f]
NH Oceans	0	0.143[f]	0.857[f]
SH Ocean	0	0.143[f]	0.857[f]
Polar	0	0.143[f]	0.857[f]
Midtroposphere	0	0.143[f]	0.857[f]
	$Fe_2O_3(s)$		
Continental	0	0.332[f]	0.668[f]
NH Oceans	0	0.332[f]	0.668[f]
SH Ocean	0	0.332[f]	0.668[f]
Polar	0	0.332[f]	0.668[f]
Midtroposphere		0.332[f]	0.668[f]

[a]Averaged from *Berner et al.* [1996], Table 2.
[b]Nucleation mode concentrations for continents were scaled with the nucleation: accumulation-mode volume concentration ratio from the continental distribution of *Whitby* [1978]. Those for ocean, polar, and upper tropospheric environments were scaled with the nucleation:accumulation-mode volume concentration ratio for marine environments from the same source.
[c]Obtained from Southern California Air Quality Study data over land sites
[d]Nss-SO_4^{2-} from Table 3
[e]Estimate
[f]*Chow et al.* [1994]
[g]Obtained from Southern California Air Quality Study data over an island site

Table 3. Mean Boundary Layer Composition of Sea-Spray Aerosols

	Northern Hemisphere		Southern Hemisphere	
Ion	< 1 um	≥ 1 um	< 1 um	≥ 1 um
Na^+	0.12	2.41	0.17	2.44
Ca^{2+}	0.055	0.49	0.026	0.24
Mg^{2+}	0.033	0.33	0.033	0.40
K^+	0.016	0.13	0.010	0.11
NH_4^+	0.12	0.0	0.04	0.001
Cl^-	0.14	4.92	0.26	4.27
nssSO_4^{2-}	0.99	0.18	0.31	0.075
ssSO_4^{2-}	0.031	0.61	0.042	0.62
NO_3^-	0.011	0.18	0.009	0.092
Br^-	0.006	0.003	0.001	0.006

Units are μg m^{-3}. Values are from data compiled by *Quinn et al.* [1998]. Size regimes refer to particle dry diameter.

bins. Concentrations in each bin were then interpolated between the boundary layer and upper troposphere. Once sulfate fields were obtained, ammonium was initialized in each size bin assuming an ammonium:sulfate mole ratio of unity.

Table 1 shows the initial globally and annually averaged burdens of individual aerosol components, before equilibrium calculations. The burden of natural plus anthropogenic tropospheric SO_4^{2-} was 2.23 Tg (0.73-Tg S), close to that of *Adams et al.* [1999] (0.70-Tg S) and between those of *Chin et al.* [1996] (0.53-Tg S) and *Lelieveld et al.* [1997] (1.05-Tg S). The tropospheric NH_4^+ burden was 0.41 Tg-NH_4^+, close to that of Adams et al. (0.39 Tg-NH_4^+). The BC burden, 0.23 Tg, was within the range of *Cooke et al.*'s [1999] estimate (0.15-0.25 Tg). The NO_3^- burden was 0.38 Tg-NO_3^-, between those of *Adams et al.* [1999] (0.13 Tg-NO_3^-) and *Andreae* [1995] (0.5 Tg-NO_3^-). The dry soil loading here was 15.1 Tg, which compares with 16.4 Tg from *Andreae* [1995] and 18.5 Tg from *Tegen et al.* [1997]. The dry sea-spray loading here was 3.3 Tg. The water content associated with sea spray was about 12 Tg when an internal mixture was assumed and 15 Tg when an external mixture was assumed, giving a global sea-spray burden of 15-18 Tg. The sea-spray burden from *Tegen et al.* [1997] was 11.4 Tg. The tropospheric plus stratospheric aerosol dry mass here was 25.1 Tg. The mass of liquid water in equilibrium with all internally-mixed aerosol components was 29.5 Tg.

2.4. Radiation

Radiative forcing calculations require aerosol, RH, temperature, and cloud fields. Temperatures, RH, and cloud fields were obtained from the time simulation. Predicted cloud liquid and ice contents were combined with modified-gamma size distribution data from *Welch et al.* [1980] and power-law/Marshall-Palmer distribution data from *Platt* [1997] for different cloud types to estimate cloud liquid and ice concentrations versus size.

Absorption, scattering, and forward scattering efficiencies for each particle size, wavelength, and core and shell refractive index were calculated with a Mie code for stratified spheres [*Toon and Ackerman*, 1981]. Cores of the stratified spheres were assumed to consist of BC. Shell refractive indices were obtained by taking volume-averages of the refractive indices of nonsolution and non-BC substances and volume-averaging these with the solution refractive index. The solution real refractive index was obtained with a partial molal refraction approach [e.g., *Stelson*, 1990; *Tang*, 1997], which requires partial molar refraction data of either ions or aqueous electrolytes, available for visible wavelengths from both references. Here, ions were combined into hypothetical

aqueous electrolytes and partial molar refractions of electrolytes were applied. Although the ion and aqueous electrolyte methods give nearly identical results, the electrolyte method was chosen, since it allows an estimate of refractive indices at nonvisible wavelengths, where partial molar refraction data are not available. At such wavelengths, partial molar refractions of aqueous electrolytes were estimated to equal those of the corresponding solid electrolyte, which appears relatively accurate [*Stelson*, 1990, Figure 1]. The solution imaginary refractive index was also calculated with a partial molar refraction approach that simplifies to a mixing rule similar to the volume-average mixing rule, except that, in the imaginary case, the index of each component in the mixture was scaled by the ratio of the solution density to the weighted sum of the densities of the individual electrolytes plus water in solution instead of by the volume fraction of the species in solution.

Table 1 indicates that, of the 47 species simulated, all 13 ions were combined into hypothetical electrolytes for partial molar refraction calculations. Wavelength-dependent UV, visible, and IR refractive indices were obtained for 30 of the remaining 34 species. Real and imaginary refractive index data for SiO_2(s), Fe_2O_3(s), and BC were obtained from Table 1.11 of *Krekov* [1993]. The midvisible refractive index value used for BC was m=1.8-0.74i. The imaginary component was between that of *Bergstrom* [1973] (m=2.0-0.66i) and *Hänel* [1987] (m=1.9-1.0i). The sensitivity of BC forcing due to the assumption of refractive index is reported by *Jacobson* [2000, Table 1]. For four species, refractive index data were not available and were estimated by combining partial molar refractions of ions constituting the species, then applying equations from *Tang* [1997] to convert partial molar refractions to refractive indices.

Once equilibrium composition and gas, aerosol, and cloud optical properties were calculated, irradiances were determined for 86, 67, and 256 wavelength intervals <0.8, 0.8-4.5, and 4.5-1000 μm, respectively (409 intervals total), with the radiative transfer algorithm described by *Toon et al.* [1989], which is integrated into the GATORG model.

In the base simulation, UV absorption by OM was accounted for. Reductions in UV irradiance of 50-75% have been observed over large biomass-burning regions [*Herman et al.*, 1999; *Krotkov et al.*, 1998]. Such plumes contain OM, certain types of which are strong UV absorbers. Known UVA and UVB-absorbing aerosol OM include nitrated aromatics, benzaldehydes, benzoic acids, aromatic polycarboxylic acids, phenols, and polycyclic aromatic hydrocarbons (PAHs) [*Jacobson*, 1999b]. Absorbing PAHs, in particular, are present in biomass-burning aerosols [*Reid et al.*, 1998; *Ferek et al.*, 1998; *Andreae et al.*, 1998; *Fang et al.*, 1999].

To account for UV reductions by OM from biomass burning and fossil fuel combustion, total OM in each model size bin was divided into three types of OM, each with different optical characteristics: 10% was assumed to consist of compounds, such as PAHs and nitrated aromatics, that strongly absorb UV radiation (OM3), 40% was assumed to consist of compounds, such as benzaldehdyes, that weakly-to-moderately absorb UV (OM2), and the rest was assumed to absorb UV only slightly (OM1). Wavelength-dependent imaginary refractive indices of OM3 were assumed to be an average of the refractive indices of 4-nitrophenol and the 4-nitrophenol anion and those of OM2 were assumed to be an average of the refractive indices of 2-hydroxybenzaldehyde and 3-nitrophenol. Indices for all these species are shown in Figure 2 of *Jacobson* [1999b].

O'*Brien et al.* [1975] and *Mylonas et al.* [1991] found that organic nitrates made up 12-21% of organic mass in Los Angeles. The estimate that 10% of global-scale OM contains strongly-absorbing nitrated organics or PAHs is less than the percent of nitrated organics measured in Los Angeles. The OM size distribution parameters here (Table 2a) for the nucleation mode were from tunnel-study OM data [*Venkataraman et al.*, 1994]. Those for other modes were taken from ambient data [*Berner et al.*, 1996]. OM was treated as a shell material for optical calculations.

Forcing calculations of individual ions (NH_4^+, Na^+, Mg^{2+}, Ca^{2+}, K^+, NO_3^-, Cl^-) and families of ions/undissociated electrolytes, including the S(VI) family [H_2SO_4(aq) HSO_4^-, and SO_4^{2-}], were determined by running a simulation with all components present, then running a simulation after removing an individual ion or family. Upon removal of the ion or family, charge was automatically adjusted in each size bin to ensure initial charge neutrality. For consistency, adjustments for anions (cations) were treated in the same way as those for all other anions (cations). If an anion [e.g., S(VI), NO_3^-, Cl^-] was removed, H^+ was first reduced. If the initial anion molality exceeded that of H^+, H^+ was reduced to a minimum value and CO_3^{2-} was added until initial charge balance was obtained. If a cation [e.g., Na^+, NH_4^+, Ca^{2+}, Mg^{2+}, K^+] was removed, H^+ was increased until charge balance occurred. In both cases, H^+, CO_3^{2-}, and all other ion molalities changed during subsequent equilibrium calculations. When ions were removed, solution compositions and LWCs changed, affecting forcing. Although other methods of balancing charge are possible for individual ions, the methods above were chosen so that they could be applied uniformly to all cations and anions. Following initialization, charge- and mass-conserving equilibrium calculations were performed to predict equilibrium composition.

The purpose of calculating forcing due to natural aerosol constituents is to estimate the relative importance of such constituents in the global radiative balance. If, for example, sea spray or natural soil has a sufficient forcing, it should be included in the diabatic heating rate term of global models. The purpose of calculating forcing due to natural ions, such as natural chloride and sulfate, is to maintain consistency with calculations of anthropogenic sulfate, nitrate, and ammonium forcing. An alternative to removing ions is to remove electrolytes (e.g., Na^+/Cl^-), but this technique creates charge-balance issues, since, for example, Na^+ does not balance Cl^- in sea spray.

3. Model Comparisons With Observations

3.1. Global Radiative and Cloud Parameters

Table 4 compares modeled globally and annually averaged TOA (defined at 0.425 mb) irradiances, TOA cloud forcings, surface irradiances, cloud fraction, and precipitation with observations. The observed cloud forcing, derived by *Kiehl et al.* [1998] and *Hack et al.* [1998] from the Earth Radiation Budget Experiment, was about -19.0 W m^{-2}. GATORG cloud forcing was about -20.0 W m^{-2}. Figure 1 compares December-January-February (DJF) and June-July-August (JJA) GATORG predictions of zonally averaged cloud fraction with Nimbus-7 satellite data from *Hack et al.* [1998, Figure 13]. The figure suggests that the JJA predictions were consistent with observations, except for overpredictions at midlatitudes in the Northern Hemisphere. The DJF predictions were also

Table 4. Comparison of GATORG Predictions, Averaged Globally Over the 24 Simulations, With Observed Globally and Annually Averaged Radiative and Cloud Properties

	Observed	Predicted
TOA thermal-IR irradiance, W m^{-2} (- is up)		
with gases, with aerosols, with clouds	-234.8[a]	-230.1
with gases, with aerosols, no clouds	-264.0[a]	-260.6
TOA solar irradiance, W m^{-2} (+ is down)		
with gases, with aerosols, with clouds	+238.1[a]	+240.1
with gases, with aerosols, no clouds	+286.3[a]	+290.6
TOA thermal-IR cloud forcing, W m^{-2}	+29.2[a]	+30.5
TOA solar cloud forcing, W m^{-2}	-48.2[a]	-50.5
TOA total cloud forcing, W m^{-2}	-19.0[a]	-20.0
Surface thermal-IR with clouds, W m^{-2}	-66.0[b]	-59.3
Surface solar irradiance with clouds, W m^{-2}	+168.0[b]	+161.3
Total cloud fraction, %	52.2-62.5[a]	61.9
Precipitation rate, mm d^{-1}	2.69[c]	2.81

[a]*Kiehl et al.* [1998]
[b]*Kiehl and Trenberth*[1997]
[c]*Xie and Arkin* [1996]

consistent in the Southern Hemisphere but were high in the Northern Hemisphere. Errors in Northern-Hemisphere cloud predictions may have been due to excess convection and water vapor predicted in the model, possibly due to errors in treating convection over heterogeneous topography with coarse grid spacing. *Hack et al.* [1998, Figure 13] shows that predictions from the Community Climate Model (CCM3) were similarly high in the Northern Hemisphere for DJF.

3.2. Aerosol Optical Parameters

Plate 1a shows the modeled yearly-averaged spatial distribution of the near-surface aerosol optical depth at 550 nm. Plates 1b and 1c show the corresponding near-surface total aerosol wet mass and aerosol LWC, respectively. Global- and hemispheric-average values of optical depth and other parameters are given in Table 5. Modeled midvisible single-scattering albedos (0.86-0.95) and optical depths (0.1-0.4) over the eastern United States and western Atlantic Ocean are within the range of measured values from TARFOX, given as 0.89-0.93 and 0.06-0.55, respectively [*Russell et al.*, 1999a, 1999b; *Hignett et al.*, 1999]. *Bergstrom and Russell* [1999] estimated the annual average aerosol radiative flux change under all-sky conditions due to all natural and anthropogenic

Table 5. Modeled Annually Averaged Values of Several Parameters

Parameter	Globe	SH	NH	Land	Sea
ω_0 at 550 nm	0.91	0.94	0.89	0.85	0.93
g_0 at 550 nm	0.70	0.71	0.68	0.64	0.72
τ_{aer} at 550 nm	0.14	0.10	0.18	0.16	0.13
0-km LWC	8.1	7.4	8.7	4.1	9.6
5-km LWC	0.58	0.73	0.43	0.28	0.69
0-km aerosol wet mass	32	20	44	45	27
5-km aerosol wet mass	0.78	0.97	0.58	0.38	0.93

SH is Southern Hemisphere, NH is Northern Hemisphere. Variable ω_0 is the near-surface single-scattering albedo, g_0 is the near-surface asymmetry parameter, and τ_{aer} is the aerosol optical depth. Liquid water content (LWC) and wet masses are in units of $\mu g\ m^{-3}$.

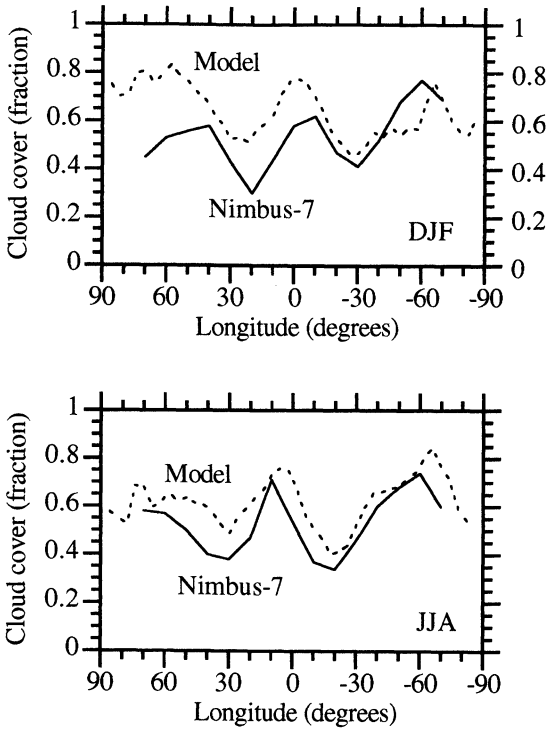

Figure 1. Comparison of December-January-February (DJF) and June-July-August (JJA) GATORG predictions of zonally averaged Nimbus 7 satellite cloud fraction data, obtained from *Hack et al.* [1998, Figure 13].

aerosol components from TARFOX data over the North Atlantic as -0.8 to -1.1 W m^{-2}. Base-case flux changes over the North Atlantic from this work under the same conditions were about -1.1 W m^{-2}. Their June-July-August flux change for all aerosols over the North Atlantic under clear-sky conditions was -5.1 W m^{-2}, which compares with -4.7 W m^{-2} calculated here.

Modeled annually averaged midvisible optical depths over the global oceans were calculated here as 0.13 (Table 5), which compares well with a mean value of 0.12 obtained from advanced very high resolution radiometer (AVHRR) data by *Husar et al.* [1997], although some spatial differences are evident. The yearly-averaged modeled optical depth of the aerosol plume over the ocean to the west of the Sahara desert, observed in AVHRR data, was about 0.2-0.33, which compares with an annual value of near 0.4-0.5 estimated from *Husar et al.* [1997]. Model errors were likely due to underestimates of the concentration of elevated soil dust.

Table 6. Comparison of Base-Case Predicted Single-Scattering Albedos With Annual Average Measurements[a]

Location	Predicted	Observed
Barrow (71.2 °N, 156.3 °W)	0.97	0.96
Amundsen Scott (90 °S)	0.97	0.965
Ny Alesund (79 °N, 12 °E)	0.90	0.948
Arctic	0.94	0.96
Mesa Verde (37.1 °N, 108.3 °W)	0.87	0.91
Abastumani (41.4 °N, 42.5 °E)	0.84	0.89
Anderson Mesa (35.12 °N, 111.38 °W)	0.89	0.94

[a]*Heintzenberg et al.* [1997]

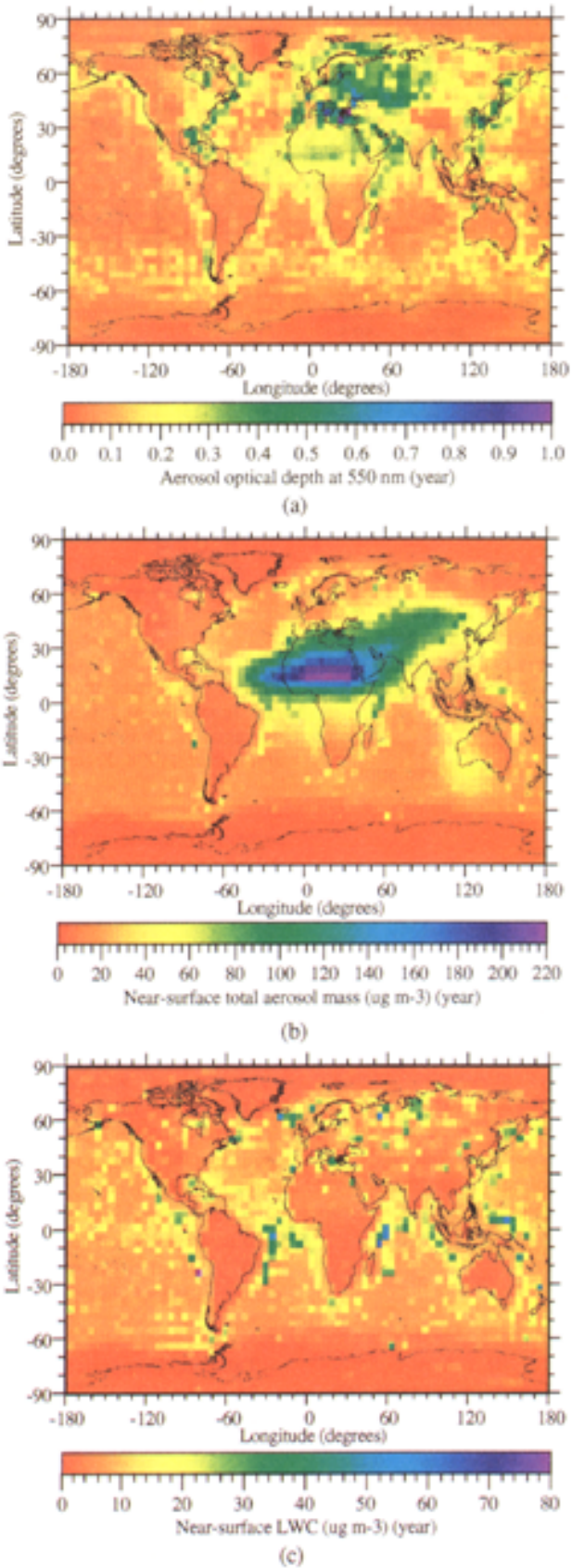

Plate 1. Modeled global distributions of (a) annually averaged stratopause to surface total aerosol optical depth at 550 nm, (b) annually averaged near-surface total aerosol wet mass, integrated over all sizes, and (c) annually averaged near-surface aerosol liquid water content, integrated over all sizes.

Modeled optical depths in the Arabian Sea (0.15-0.45) and Indian Ocean (0.05-0.15) at 550 nm, shown in Plate 1a, were within the range of values observed during the Indian Ocean Experiment (INDOEX) by *Jayaraman et al.* [1998], given as 0.2-0.4 and ≤0.1, respectively.

Table 6 compares aerosol single-scattering albedos calculated from the base-case simulation (BC treated as core) with annual average observations at several locations [*Heintzenberg et al.*, 1997]. The results indicate agreement to within <7% in all cases, less than the error of the measurements. *Hitzenberger and Puxbaum* [1993] found absorption coefficient measurement errors of +15-20% during high pollution episodes but >+200% for background atmospheric absorption. All single-scattering albedo observations, except for one, were at relatively clean locations.

4. Aerosol Composition, Mass, and LWC

Figure 2 shows modeled vertical profiles of globally and yearly averaged aerosol composition from the simulations. Figure 2a, which shows profiles of sulfate-containing compounds and water, indicates that gypsum ($CaSO_4$-$2H_2O$) was the most abundant sulfate-containing solid in the atmosphere. This is not surprising, since its DRH is 98%, allowing it to form in sea spray drops, which contain both calcium and sulfate, and in soil dust, which contains calcium and become acidified upon sulfuric-acid condensation. Despite its abundance, gypsum plays a relatively small role in the global radiative balance, since it forms primarily in the coarse-particle mode. When gypsum was not allowed to form in the model, the direct forcing due to all aerosols was only 0.01 W m^{-2} more negative than when it was allowed to form.

Thenardite (Na_2SO_4, DRH=84.2%) and arcanite (K_2SO_4, DRH=97.5%) were estimated to be the next most common sulfate-salts. Since both are present primarily in the coarse mode (Na^+ and K^+ are both present in sea spray and soil), they also have relatively little radiative effect. Ammonium bisulfate (NH_4HSO_4, DRH=40%) and mascagnite [$(NH4)_2SO_4$, DRH=80%], often assumed to be the main solid forms of sulfate, were estimated to be the fourth and fifth most-common sulfate salts. Of the total sulfate initialized in the model, about 14% precipitated and the rest remained aqueous.

The most common ammonium salt (Figure 2b) was sal ammoniac (NH_4Cl, DRH=77.1%), formed from dissolved ammonia and sea-spray chloride. Halite (NaCl, DRH=75.3%) was the most abundant sodium and chloride-containing salt (Figures 2c and 2d). Nitrum (KNO_3, DRH=92.5%), which forms when nitric acid enters sea-spray or soil-dust particles, was the most common nitrate salt (Figure 2d). Calcite ($CaCO_3$, DRH=100%) and magnesite ($MgCO_3$, DRH=100%), present in soil dust, were the most common calcium and magnesium salts, respectively (Figure 2e).

Aerosol wet mass is the sum of dry mass and liquid water. The effect of modeled RH on aerosol LWC was discussed in Section 2.2. Table 5 indicates that near-surface aerosol wet mass was higher in the Northern Hemisphere (near 44 μg m^{-3}) than in the Southern Hemisphere (near 20 μg m^{-3}) and over land (near 45 μg m^{-3}) than over the oceans (near 27 μg m^{-3}). Both results were expected, since loadings of soil dust, which makes up most aerosol mass, were higher in the Northern Hemisphere and over land than in the Southern Hemisphere and over the oceans, respectively. Table 5 also shows that near-surface aerosol LWCs were similar in the Northern and Southern Hemispheres (near 7-9 μg m^{-3}), but higher over the oceans (near 10 μg m^{-3}) than over land (near 4 μg m^{-3}).

As shown in Plate 1b, the highest concentration of total aerosol wet mass was over North Africa, where Sahara dust is present. Corresponding aerosol LWCs were low in that region (Plate 1c). Aerosol LWCs over the oceans sometimes reached 20-40 μg m^{-3}, but were more frequently 5-25 μg m^{-3}. Over land, LWCs were commonly below 10 μg m^{-3}, but were relatively high (up to 40 μg m^{-3}) in regions of high sulfate concentrations.

5. Baseline Aerosol Forcing Results

Table 7 shows predictions of near surface, tropopause, and TOA aerosol direct forcing, averaged over the 24 simulations and globally. The table also compares tropopause forcing over the Northern versus Southern Hemispheres and over land versus ocean. Table 8 compares modeled tropopause forcings from Table 7 with those from previous studies. Figure 3 shows the modeled globally averaged tropopause forcings in bar-graph form.

5.1. Sea-Spray Forcing

Sea spray covers 2/3 of the Earth's surface. Table 7 shows that, on a global scale, modeled yearly-averaged sea-spray forcing was -0.55 W m^{-2} at the tropopause in the presence of clouds and -1.1 W m^{-2} at the TOA in the absence of clouds. These forcings were greater in magnitude than those due to natural sulfate and natural soil under clear and cloudy conditions, making sea spray the most important natural aerosol constituent in the atmosphere in terms of direct forcing.

The baseline sea-spray forcing was obtained with sea spray mixed with soil, sulfate, and other material as a shell component in particles. A sensitivity test was run to calculate sea spray forcing when it was treated as externally-mixed. When externally-mixed, sea-spray forcing was -0.67 W m^{-2} (versus -0.55 W m^{-2} for an internal mixture). When sea spray was externally-mixed, ammonium and nss-sulfate were excluded from sea-spray particles, resulting in lower concentrations of solids (particularly $CaSO_4$-$2H_2O$ and NH_4Cl) and greater LWCs. Greater LWCs in the external-mixture case were also caused by the fact that Na^+/Cl^- hydrates more liquid water than does NH_4^+/Cl^- at the same RH.

Table 7 shows that chloride and its associated liquid water caused a tropopause forcing of -0.29 W m^{-2}, close to that of natural sulfate (-0.34 W m^{-2}). Chloride's concentrations over noncoastal ocean regions (where acidification is small in the coarse mode) are 1-12 μg m^{-3}, with an average value of about 4.8 μg m^{-3} [*Quinn et al.*, 1998]. Average continental concentrations of Cl^- are only about 0.15 μg m^{-3} [*Pueschel*, 1995]. Near 5.5 km, Cl^- concentrations may range from 0.0085 to 0.02 μg m^{-3} [*Talbot et al.*, 1998; *Li et al.*, 1997].

5.2. BC Forcing

Table 7 shows that the modeled all-sky, globally and yearly averaged tropopause base-case forcing due to anthropogenic (total) BC from fossil fuels and biomass burning was +0.53 W m^{-2}. This estimate was obtained by treating BC as core material in an internal mixture for radiative calculations. When BC was treated as externally-mixed instead of as core material, its forcing was cut in half, to +0.27 W m^{-2}. When the refractive

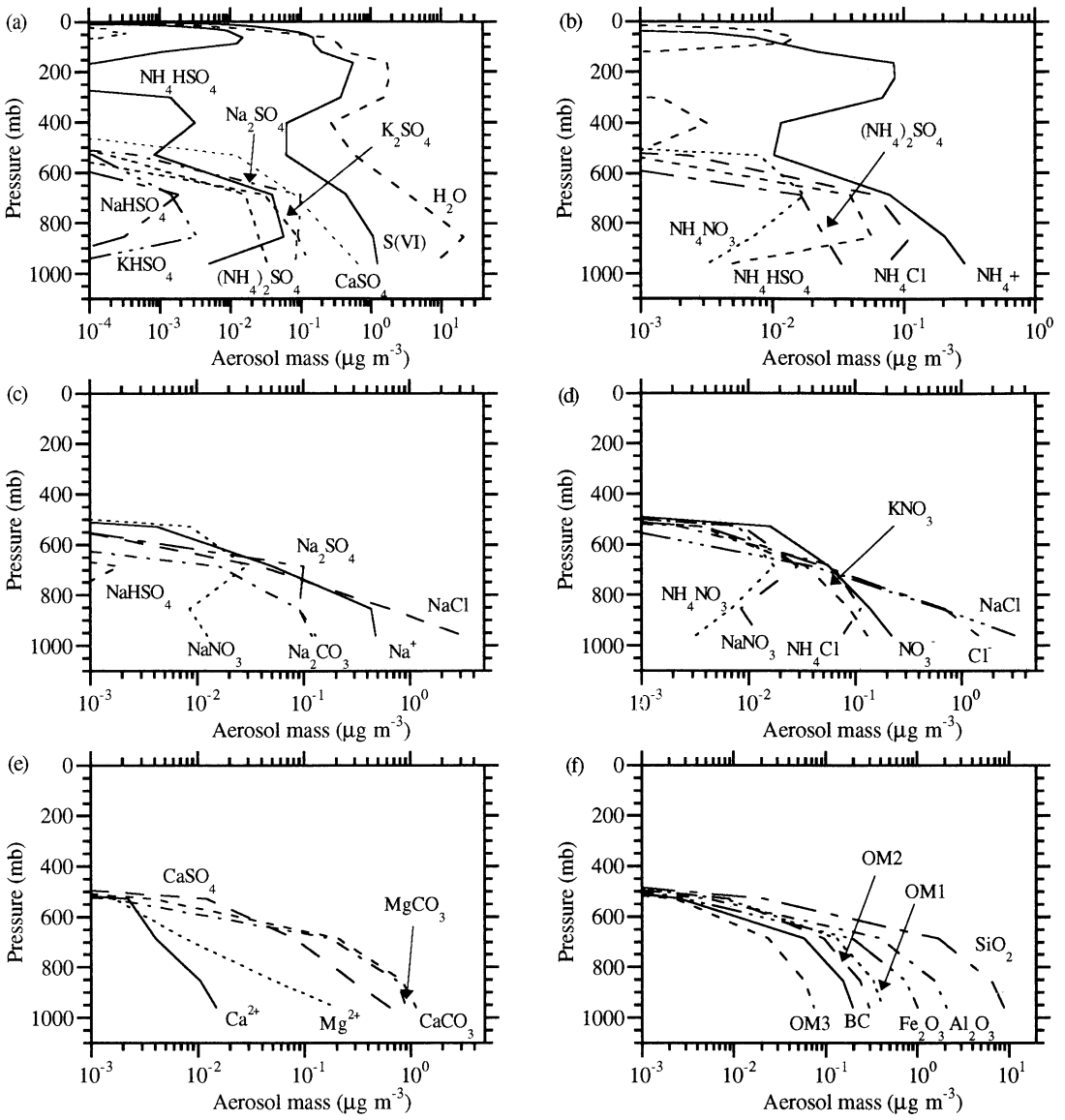

Figure 2. Modeled globally and yearly averaged vertical profiles of (a) sulfate, its salts, and water, (b) ammonium and its salts, (c) sodium and its salts, (d) nitrate, chloride and their salts, (e) calcium, magnesium, and their salts, and (f) BC, OM, and insoluble soil compounds.

indices of BC were volume averaged with those of other components in an internal mixture, BC forcing increased to +0.78 W m^{-2}. The reason for using the core treatment over the external- or well-mixed internal treatment is discussed by *Jacobson* [2000].

5.3. Sulfate, Ammonium, and Nitrate Forcing

Table 7 shows that the modeled all-sky, globally and yearly averaged tropopause base-case forcing due to anthropogenic sulfate was -0.32 W m^{-2}. This compares with the Intergovernmental Panel on Climate Change (*IPCC*) [1996] estimate of -0.4 (-0.2 to -0.8) W m^{-2}.

Here, modeled natural sulfate tropopause forcing was -0.34 W m^{-2}. Modeled TOA sulfate forcing in the absence of clouds was about 1.8 times more negative than that in the presence of clouds. Thus, clouds decreased the magnitude of negative sulfate forcing.

The baseline anthropogenic sulfate forcing estimate was obtained with sulfate internally-mixed as a shell component. A test was run to calculate its forcing when it was treated as externally-mixed. When externally-mixed, anthropogenic sulfate forcing was -0.53 W m^{-2} (versus -0.32 W m^{-2} when internally-mixed). In the external-mixture case, sulfate's charge was balanced by H^+ alone. In the internal-mixture case, its charge in submicron particles was balanced primarily by NH_4^+. At the same RH, $2NH_4^+/SO_4^{2-}$ and NH_4^+/HSO_4^{2-} hydrate less water than do H^+/HSO_4^- or $2H^+/SO_4^{2-}$, causing the lesser negative forcing when sulfate was internally-mixed than when it was externally-mixed.

The anthropogenic and total ammonium tropopause forcings in Table 7 were +0.06 and +0.11 W m^{-2}, respectively. The positive forcing due to ammonium indicates that it contributes to climate warming. The reason for the positive forcing is that, in the absence of ammonium, sulfate charge is balanced

Table 7. Modeled Surface, Tropopause, and TOA Solar Plus Thermal-IR Direct Forcing (W m^{-2}), Averaged Over the 24 Simulations, for All Aerosols Except Specified Components (Except in the Case of "All aerosols", Where the Forcing is Due to All Aerosol Constituents)

	With clouds										No clouds	
	Surface	Tropopause, 227 mbar, 11 km-									TOA, 0.425 mbar 55 km	
	Global Baseline	Global Baseline	SH Baseline	NH Baseline	Land Baseline	Ocean Baseline	Global +15% RH	Global -15% RH	Global +50% Conc.	Global -50% Conc.	Global Baseline	Global Baseline
Natural Plus Anthropogenic Aerosols												
All aerosols	-4.0	-1.37	-1.29	-1.44	-0.73	-1.62	-2.62	-0.51	-1.99	-0.71	-1.23	-2.48
All soil dust[b]	-0.85	-0.13	-0.05	-0.21	-0.11	-0.14	-0.15	-0.09	-0.19	-0.07	-0.14	-0.23
All sea-spray drops[c]	-0.54	-0.55	-0.68	-0.41	-0.08	-0.73	-0.99	-0.22	-0.80	-0.29	-0.54	-1.1
All S(VI)	-0.73	-0.66	-0.44	-0.87	-0.86	-0.58	-1.0	-0.37	-0.95	-0.34	-0.52	-0.94
All tropospheric S(VI)	-0.45	-0.45	-0.20	-0.68	-0.69	-0.35	-0.68	-0.24	-0.64	-0.23	-0.44	-0.84
All stratospheric S(VI)	-0.28	-0.21	-0.24	-.19	-0.17	-0.23	-0.32	-0.13	-0.31	-0.11	-0.08	-0.10
All natural S(VI)	-0.40	-0.34	-0.31	-0.36	-0.31	-0.35	-0.51	-0.19	-0.49	-0.17	-0.21	-0.41
All NH_4^+	+0.12	+0.11	+0.07	+0.15	+0.15	+0.09	+0.15	+0.03	+0.17	+0.06	+0.10	+0.21
All Na^+, Na_2CO_3	+0.04	+0.07	+0.09	+0.05	+0.001	+0.10	+0.26	+0.02	+0.10	+0.04	+0.07	+0.09
All K^+, K_2CO_3	-0.02	-0.002	-0.003	-0.001	+0.002	-0.004	-0.002	-0.002	-0.003	-0.001	-0.003	-0.008
All Ca^{2+}, $CaCO_3$	-0.03	+0.02	+0.02	+0.01	+0.006	+0.02	+0.02	+0.02	+0.03	+0.01	+0.02	+0.034
All Mg^{2+}, $MgCO_3$	-0.042	+0.005	+0.009	+0.001	+0.007	+0.004	+0.005	+0.005	+0.008	+0.003	+0.005	+0.03
All NO_3^-	-0.07	-0.07	-0.07	-0.08	-0.10	-0.06	-0.11	-0.03	-0.11	-0.04	-0.07	-0.12
All Cl^-	-0.23	-0.29	-0.35	-0.23	-0.03	-0.39	-0.54	-0.12	-0.42	-0.15	-0.28	-0.51
All OM	-0.35	-0.063	-0.06	-0.07	-0.13	-0.04	-0.06	-0.06	-0.09	-0.03	-0.07	-0.12
All SiO_2	-0.27	-0.17	-0.06	-0.27	-0.29	-0.12	-0.17	-0.17	-0.26	-0.08	-0.17	-0.25
All Al_2O_3	-0.19	+0.06	+0.02	+0.11	+0.18	+0.02	+0.06	+0.06	+0.09	+0.03	+0.06	+0.062
All Fe_2O_3	-0.30	+0.002	-0.001	+0.006	+0.04	-0.01	+0.002	+0.002	+0.003	+0.001	+0.002	-0.02
Anthropogenic Aerosols												
All anthropogenic[d]	-2.5	-0.12	-0.08	-0.16	+0.18	-0.24	-0.19	+0.06	-0.20	-0.05	-0.13	-0.89
Anthropogenic soil dust[e]	-0.41	-0.07	-0.03	-0.12	-0.08	-0.07	-0.08	-0.05	-0.10	-0.04	-0.08	-0.15
Anthropogenic S(VI)[f]	-0.33	-0.32	-0.13	-0.51	-0.55	-0.23	-0.49	-0.18	-0.46	-0.17	-0.31	-0.53
Anthropogenic BC, fossil fuels and biomass burning[g]	-1.4	+0.53	+0.26	+0.80	+1.23	+0.25	+0.55	+0.49	+0.78	+0.27	+0.52	+0.50
Anthropogenic OM, fossil fuels and biomass burning[h]	-0.32	-0.057	-0.05	-0.06	-0.12	-0.03	-0.06	-0.06	-0.08	-0.03	-0.06	-0.11
Anthropogenic NH_4^+ [i]	+0.06	+0.06	+0.04	+0.08	+0.08	+0.05	+0.08	+0.02	+0.08	+0.03	+0.05	+0.12
Anthropogenic NO_3^- [j]	-0.04	-0.05	-0.04	-0.05	-0.06	-0.04	-0.07	-0.02	-0.07	-0.03	-0.04	-0.08

[a]SH is Southern Hemisphere, NH is Northern Hemisphere, RH is relative humidity. Forcing when clouds are present is calculated as $F_{g,a,c}\downarrow - F_{g,a-x,c}\downarrow$, where $F\downarrow$ is net downward (downward-upward) irradiance (W m^{-2}), the subscript g indicates with all gases present, the subscript a indicates with all aerosols present, the subscript c indicates with clouds present, the subscript a-x indicates with all aerosols, except for the component of interest, present, and the subscript x alone indicates with no aerosols, except the component of interest, present. Forcing in the absence of clouds is calculated as $F_{g,a}\downarrow - F_{g,a-x}\downarrow$. A positive number indicates a net warming influence. The first two sensitivity columns (±15% RH) account for the sensitivity of the base-case forcing to changes in RH of ±15% (with an upper limit of 99% RH), and the next two columns (±50% Conc.) account for the sensitivity to changes in the concentrations of all aerosol components simultaneously of ±50%.

[b]SiO_2, Al_2O_3, Fe_2O_3, $CaCO_3$, $MgCO_3$, K_2CO_3, Na_2CO_3, and associated H_2O(aq).

[c]Na^+, K^+, Ca^{2+}, Mg^{2+}, Cl^-, S(VI) from sea-spray drops and associated H_2O(aq).

[d]All anthropogenic aerosols include 70% of S(VI) <1 μm in diameter [*Langner and Rodhe*, 1991], 63% of NO_3^- [*Andreae*, 1995, Table 2], 50% of NH_4^+ (estimate), all BC, 90% of OM [*Liousse et al.*, 1996, Table 1], and 50% of soil dust [*Tegen et al.*, 1996].

[e]50% of all soil dust [*Tegen et al.*, 1996].

[f]70% of tropospheric S(VI) <1 μm in diameter [*Langner and Rodhe*, 1991].

[g]100% of BC.

[h]90% of all OM [*Liousse et al.*, 1996, Table 1].

[i]50% of all NH_4^+ (estimate).

[j]63% of all NO_3^- [*Andreae*, 1995, Table 2].

primarily by H^+. Since $2NH_4^+/SO_4^{2-}$ and NH_4^+/HSO_4^{2-} hydrate less water than do H^+/HSO_4^- or $2H^+/SO_4^{2-}$ at the same RH, the addition of ammonium to an S(VI) solution decreases liquid water content, causing positive ammonium forcing.

Table 7 shows that anthropogenic and total nitrate forcings were -0.05 and -0.07 W m^{-2}, respectively. These numbers compare with -0.04 and -0.06 W m^{-2}, respectively from *Andreae* [1995] (scaled from NH_4NO_3 forcings with the NO_3^-:NH_4NO_3 mole ratio). Like chloride and sulfate, nitrate enhances cooling.

Table 8. Comparison of Tropopause Forcings (W m^{-2}) in the Presence of Clouds From This Work With Those From Other Studies[a]

	This Work	Other Studies
	$F_{g,a,c}\downarrow - F_{g,a-x,c}\downarrow$	$F_{g,x,c}\downarrow - F_{g,c}\downarrow$
Stratospheric S(VI)	-0.21 (tropopause) -0.08 (stratopause)	-0.1[b]
All anthropogenic	-0.12	-0.5 (-0.25 to -1.0)[c]
Anthropogenic soil dust	-0.07	+0.14[d], -0.12[e], -0.08[f]
Anthropogenic S(VI)	-0.32	-0.40 (-0.2 to -0.8)[c] -1.1[g], -0.3[h], -0.95[i], -0.4[j], -0.35[k], -0.2[e], -0.6 to -0.8[l], -0.55 to -0.81[m], -0.23 to -0.34[n], -0.32[s]
Anthropogenic BC from fossil fuels and biomass burning	+0.53	from fossil fuels +0.1 (+0.03 to +0.3)[c], +0.20 to +0.36[o], +0.20[m], +0.16 to +0.42[s], +0.17[t] from fossil fuels and biomass burning +0.40[l], +0.27[p], +0.78[q]
Anthropogenic OM from fossil fuels and biomass burning	-0.06	from biomass burning -0.2 (-0.07 to -0.6)[c] from fossil fuels and biomass burning -0.22[e], -0.09[r] from fossil fuels -0.024[t]

[a]Definitions of the aerosol categories are the same as those in Table 7. Units are W m^{-2}.
[b]*Hansen et al.* [1997].
[c]*IPCC* [1996].
[d]*Tegen et al.* [1996].
[e]*Hansen et al.* [1998].
[f]*Miller and Tegen* [1998].
[g]*Charlson et al.* [1991].
[h]*Kiehl and Briegleb* [1993].
[i]*Taylor and Penner* [1994].
[j]*Chuang et al.* [1997].
[k]*Feichter et al.* [1997].
[l]*Haywood and Ramaswamy* [1998], BC externally mixed.
[m]*Penner et al.* [1998], BC externally mixed.
[n]*Boucher and Anderson* [1995].
[o]*Haywood et al.* [1997], BC externally to well-mixed internally.
[p]This work, BC externally mixed.
[q]This work, BC well-mixed internally.
[r]This work, no UV absorption by OM.
[s]*Myhre et al.* [1998], BC externally to well-mixed internally.
[t]*Cooke et al.* [1999], BC externally mixed.

5.4. OM Forcing

Table 7 shows that the modeled all-sky, globally and yearly averaged tropopause base-case forcing due to total and anthropogenic OM were -0.063 and -0.057 W m^{-2}, respectively. The OM forcing estimates did not account for OM uptake of liquid water; thus, the magnitude of OM forcing was probably underestimated although the sign should be correct (addition of water enhances negative forcing).

For comparison, *Cooke et al.* [1999] estimated OM forcing due to fossil fuels alone of -0.024 W m^{-2}. Since the biomass-burning to fossil fuel OM emissions ratio from *Liousse et al.* [1996] is about 1.6, an extrapolation of Cooke et al.'s results gives a forcing for biomass burning plus fossil fuel OM of -0.06 W m^{-2}.

When UV absorption by OM was ignored here, the total (anthropogenic) OM forcing decreased by 0.05 (0.045) W m^{-2} to -0.11 (-0.10) W m^{-2}. Since the UV absorbing properties of organics are uncertain, a conservative range of the incremental forcing due to UV absorption by organics is suggested as +0.03 to +0.05 W m^{-2}.

5.5. Soil Dust Forcing

Table 7 shows that the modeled all-sky, globally and yearly averaged tropopause base-case forcings due to total and anthropogenic soil dust were -0.13 and -0.07 W m^{-2}, respectively. The model considered seven soil-dust components, $SiO_2(s)$, $Fe_2O_3(s)$, $Al_2O_3(s)$, $Na_2CO_3(s)$, $K_2CO_3(s)$, $CaCO_3(s)$, and $MgCO_3(s)$. Much of $SiO_2(s)$'s negative solar forcing was offset by strong positive thermal-IR forcing, giving $SiO_2(s)$ a modest net forcing. $Al_2O_3(s)$ had a net positive tropopause forcing because it absorbs in the visible and UV spectra. $Fe_2O_3(s)$, which had a near-zero tropopause forcing, is a slightly stronger UV and short-visible absorber than is $Al_2O_3(s)$, but $Al_2O_3(s)$ absorbs more than does $Fe_2O_3(s)$ at long visible wavelengths. Table 8 shows that anthropogenic soil-dust forcing estimates from other studies vary from +0.14 to -0.12 W m^{-2}. The anthropogenic soil dust estimates here are within the ranges of the other estimates.

5.6. Total and Anthropogenic Aerosol Forcing

Table 7 shows that the modeled all-sky, globally and yearly averaged tropopause base-case solar plus thermal-IR forcing due to anthropogenic aerosols (-0.12 W m^{-2}) was slightly negative. The magnitudes of all anthropogenic forcing components were greater in the Northern Hemisphere than in the Southern Hemisphere and over land than over the oceans. Tropopause forcing by anthropogenic plus natural aerosols was -1.37 W m^{-2}. Table 8 shows that the *IPCC* [1996] estimate of direct forcing due to all anthropogenic aerosols ranged from -0.25 to -1.0 W m^{-2}, with a suggested value of -0.5 W m^{-2}. The base-case estimate here of -0.12 W m^{-2} is lower in magnitude than the IPCC estimate, primarily due to the treatment of BC as core [*Jacobson*, 2000], but also due to differences in other forcing constituents, as indicated in Table 8.

6. Profiles of Aerosol Forcing

Figure 4 shows modeled vertical profiles of globally and 24-simulation averaged aerosol forcings for the solar, thermal-IR, and total spectra. The base-case solar plus thermal-IR total aerosol forcing changed from -1.23 to -4.0 W m^{-2} between the TOA and surface. Total-aerosol solar forcing was negative and became more negative between the TOA and surface due to decreases in values and increases in magnitudes of forcing by BC, soil dust, and OM, all of which absorb solar radiation. Although less absorbing in the solar spectrum than BC, soil dust and OM also absorb, particularly in the UV spectrum.

Figure 4 shows that solar forcings due to sea-spray drops, chloride, and sulfate were relatively uniform with altitude. If a species is entirely nonabsorbing, irradiances are equal at all altitudes regardless of the concentration profile, and the species' forcing profile is uniform in the vertical and slightly negative (due to net backscattering). Sulfate and chloride are relatively nonabsorbing in the solar spectrum. Nevertheless,

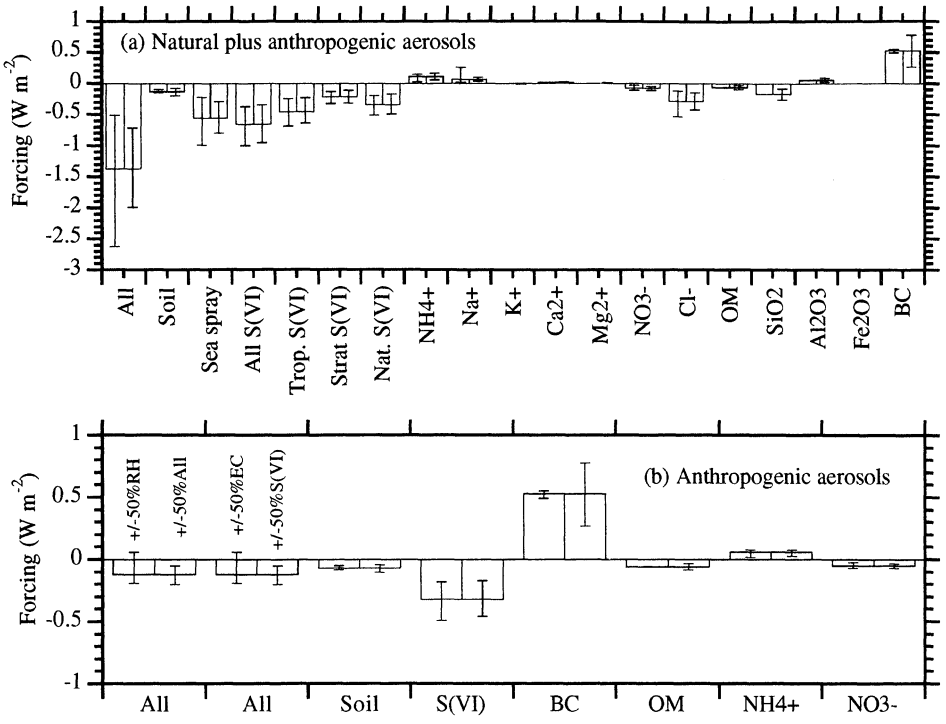

Figure 3. Modeled base-case globally and yearly averaged all-sky tropopause solar plus thermal-IR forcings (W m^{-2}) for (a) anthropogenic plus natural aerosol constituents and (b) anthropogenic aerosol constituents. For each constituent (except in the case of all-anthropogenic aerosols), two sensitivity bars are given. The first bar is the variation in forcing due to RH variations of ±15%. The second bar is the variation in forcing of the individual constituent due to changes in concentration of all constituents simultaneously of ±50%. In the case of all-anthropogenic aerosols, the third and fourth bars are variations in forcing due to a ±50% variation in the global concentration of BC and anthropogenic S(VI), respectively, alone. Base-case forcings and sensitivity bar numbers are given in Tables 7 and 9.

when they are removed from solution, aerosol composition changes, preventing their forcing profiles from being perfectly straight.

Total aerosol thermal-IR forcing was generally positive, increasing in value and magnitude between the TOA and surface. In the case of ammonium, thermal-IR forcing was negative, since sulfate particles contained less water, were smaller, and absorbed less thermal-IR when ammonium was present than when it was absent. In the case of stratospheric sulfate, positive thermal-IR forcing increased with increasing altitude, since, when sulfate was absent from the stratosphere, thermal-IR wavelengths that would otherwise be absorbed by sulfate, generally escaped to space.

Near-surface thermal-IR forcing was greatest for soil dust, sea spray, and their components. Soil-dust particles and sea-spray drops are closer in diameter to typical thermal-IR wavelengths (10 μm) than are most particles containing BC, OM, or sulfate. Particles much smaller than a given wavelength are inefficient absorbers and scatterers, and although mass absorption/scattering efficiencies decrease less rapidly with decreasing radius than do individual particle absorption/scattering efficiencies, the aggregated mass of large particles usually exceeds that of small particles, decreasing the effect of particles much smaller than the wavelength on forcing.

Plate 2 shows the modeled yearly-average (24-simulation) spatial distribution of solar plus thermal-IR all-sky tropopause forcing for several aerosol constituents. Forcing was generally strongest where concentrations were highest and cloud cover was lowest. Figure 1 shows that cloud cover was lowest at 30°N and S, where synoptic-scale high-pressure systems persist.

7. Effects of Clouds on Aerosol Forcing

The difference between the last two columns in Table 7 indicates that clouds decreased the magnitude of TOA forcing of almost all aerosol constituents. Cloud cover blocked the solar optical effects of aerosols over much of the Earth, especially over the tropics, where towering cumulonimbus and cumulus congestus clouds formed. In such cases, aerosols were exposed to less incident solar radiation, which reduced the globally averaged level of aerosol-backscattered radiation and increased the positiveness of aerosol forcing in comparison with when clouds were absent. The effect of clouds on hygroscopic-aerosol forcing was large, since when thick clouds were present, the RH was high, aerosol LWC was large, and clouds prevented hygroscopic aerosol components below them from backscattering radiation. *Liao and Seinfeld* [1998] similarly found that clouds reduced the magnitude of ammonium sulfate-particle forcing.

In the case of BC, though, forcing increased when clouds were present compared with when they were absent. When stratus were present, BC residing above or within stratus were exposed to more reflected or multiple-scattered radiation than when clouds were absent. The additional exposure allowed BC to absorb more radiation when clouds were present than when they were not, enhancing positive forcing by BC. *Haywood et*

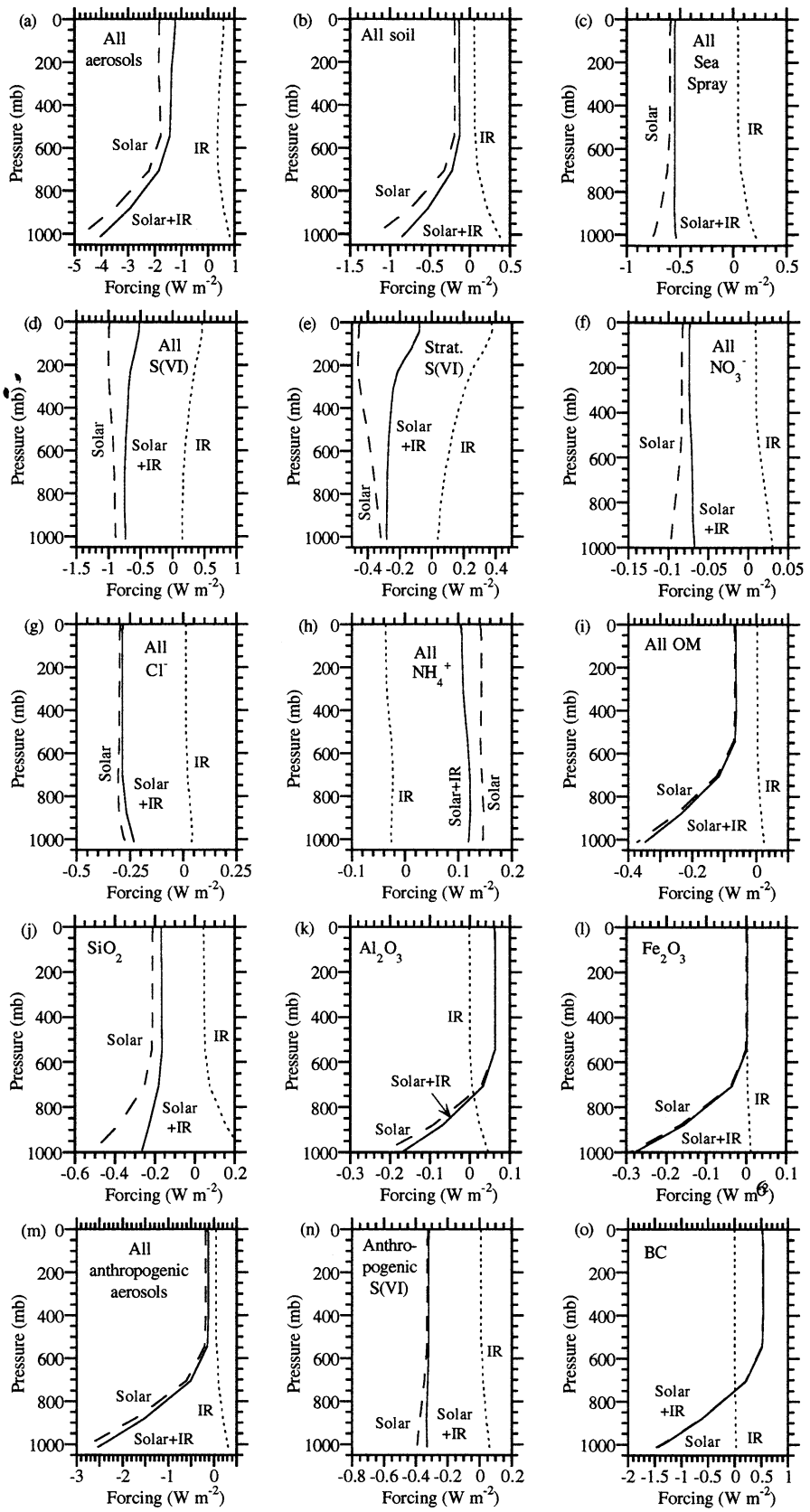

Figure 4. Modeled vertical profiles of globally and yearly averaged all-sky solar, thermal-IR, and solar plus thermal-IR direct forcing for several aerosol groups or constituents.

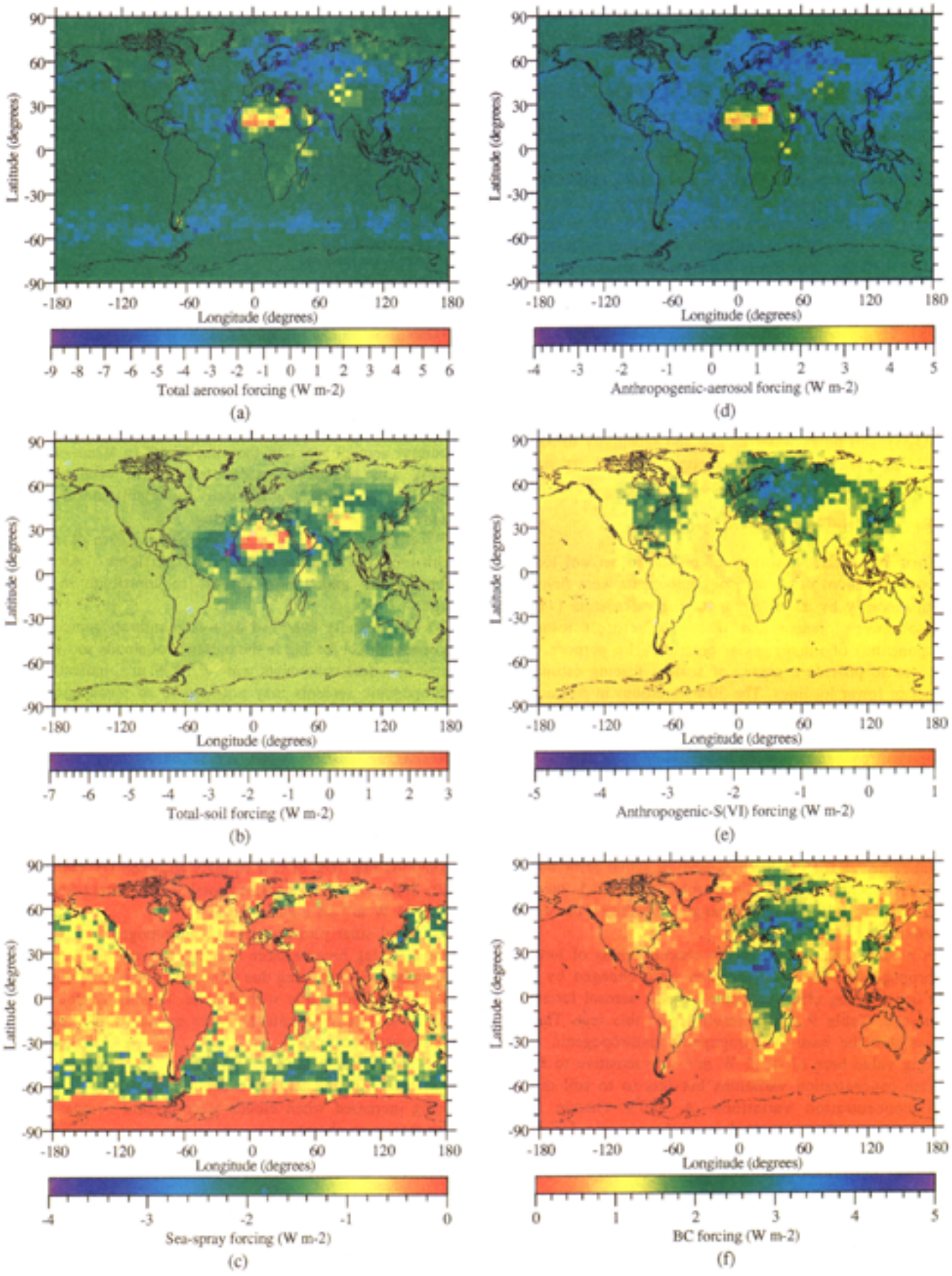

Plate 2. Modeled global distributions of yearly averaged all-sky tropopause direct forcing due to (a) total aerosols; (b) total soil; (c) sea-spray; (d) anthropogenic aerosols; (e) anthropogenic-S(VI) ; (f) BC.

al. [1998] also found that clouds enhanced absorption by BC for a similar reason.

8. Sensitivities to RH

To examine the sensitivity of forcing to RH, 3-D RH fields predicted by the model were adjusted ±15% of the RH value for equilibrium calculations. The adjusted RHs were not allowed to exceed 99%; thus, if the original RH was 90%, the ±15% sensitivity RHs were 0.85x90% and min[1.15x90%, 99%], respectively. The purpose of the sensitivity test was not to suggest that the uncertainty in RH is ±15%, but to provide a means of scaling forcing estimates to higher or lower RHs. Table 7 indicates that direct forcing was sensitive to changes in RH, as suggested previously [e.g., *Pilinis et al.*, 1995; *Nemesure et al.*, 1995; *Pilinis and Li,* 1998; *West et al.*, 1998]. Hygroscopic aerosol components, such as sulfate, nitrate, and chloride, and sea-spray drops as a whole, were more sensitive than were others, such as BC, $SiO_2(s)$, $Al_2O_3(s)$, and $Fe_2O_3(s)$. Since soil dust consists primarily of nonhygroscopic components, such as $SiO_2(s)$, $Al_2O_3(s)$, and $Fe_2O_3(s)$, soil dust's water uptake and sensitivity to RH were less than were those of hygroscopic material, as similarly suggested by *Li-Jones et al.* [1998].

9. Sensitivities to Aerosol Loadings

To examine the sensitivity of results to aerosol loadings, the concentrations of all aerosol components were first varied simultaneously by ±50% for a forcing calculation (when all aerosols were present and when all aerosols minus the component(s) of interest were present). The purpose of this test was to provide a means of scaling forcing estimates to higher or lower loadings. The 50% variations in concentration are sensitivity bounds rather than error bounds. Error bounds in the time-dependent global distribution of aerosol-component concentration are not possible to determine today, since such error estimates require knowledge of time-dependent observations over the globe, between the surface and tropopause, of each aerosol component. As such, no previous study nor compilation of studies (e.g., IPCC) of aerosol global direct radiative forcing has reported an actual error bound in global concentrations or direct forcing. Instead, they have reported sensitivity bounds or ranges of values from different simulations.

In a third sensitivity test, the concentrations of individual anthropogenic aerosol components were changed by ±50%, and the resulting effect on anthropogenic aerosol forcing was examined. Table 9 shows results from this test. The table shows that the base-case tropopause anthropogenic aerosol forcing value here of -0.12 W m^{-2} was sensitive to BC and sulfate concentration variations but less-so to soil dust and OM concentration variations. A ±50% change in BC concentration alone resulted in anthropogenic forcings of +0.06 and -0.3W m^{-2}, respectively. A ±50% change in sulfate concentration results in a anthropogenic forcings of -0.21 and -0.02 W m^{-2}, respectively.

Table 9. Mean Tropopause Anthropogenic Aerosol Forcing (W m^{-2}) in the Presence of Clouds Due to +/-50% Variations in Concentrations of Individual Anthropogenic Aerosol Components[a]

	+50% Concentration	-50% Concentration
Anthropogenic soil dust	-0.17	-0.11
Anthropogenic S(VI)	-0.21	-0.02
Anthropogenic BC from fossil fuels and biomass burning	+0.06	-0.30
Anthropogenic OM from fossil fuels and biomass burning	-0.15	-0.09

[a]Compare with baseline value of -0.12 W m^{-2} from Table 7 (the values given are forcings, not differences in forcing).

10. Summary

A global study of the solar plus thermal-IR direct forcing due to multiple anthropogenic and natural aerosols constituents was discussed. Conclusions are as follows.

(1) Gypsum was calculated to be the most common sulfate-containing salt in the global atmosphere. Sal ammoniac, halite, halite, and nitrum were the most common ammonium-, sodium-, chloride-, and nitrate-containing salts, respectively.

(2) Sea spray and BC were estimated to be the most important aerosol types in the atmosphere in terms of direct forcing and should be accounted for in climate-model predictions. Chloride was the most important natural aerosol component in terms of direct forcing.

(3) Ammonium forcing was positive, since it reduces hydration in sulfate-containing particles. As such, anthropogenic ammonium appears to contribute to global warming.

(4) The globally averaged base-case anthropogenic aerosol tropopause direct forcing in the presence of clouds and with BC treated as a core component was -0.12 W m^{-2}, indicating that anthropogenic aerosols may not lead to so much cooling as previously thought. Total natural plus anthropogenic aerosol forcing in the presence of clouds was estimated to be -1.4 W m^{-2}. Results are sensitive to RH, aerosol burdens, and the aerosol mixing state.

(5) The treatment of UV absorption by organics increased the tropopause forcing of organics (which remained negative) on a global scale by an estimated 0.03-0.05 W m^{-2} under the assumption that 10% of OM strongly absorbed UV radiation.

(6) Solid formation increased total-aerosol direct forcing by 0.03-0.05 W m^{-2} on a global scale.

(7) Total solar plus thermal-IR anthropogenic plus natural aerosol forcing became more negative between the tropopause and surface. Solar forcing due to nonabsorbing components did not change significantly with altitude. Thermal-IR forcings of soil and sea-spray constituents were greater than those of all other constituents.

(8) Clouds decreased the magnitude of TOA forcing of almost all aerosol constituents. An exception was BC. Positive BC forcing increased when clouds were present compared with when they were absent.

(9) $SiO_2(s)$ was estimated to be the dominant forcing component in soil dust. $Al_2O_3(s)$ tropopause forcing was positive.

(10) Modeled near-surface aerosol LWCs were higher over the oceans than over land.

Acknowledgments. This work was supported by grants from the Environmental Protection Agency under assistance agreement 823186-01-0, the National Science Foundation under agreements ATM-9504481 and ATM-9614118, the National Aeronautics and Space Administration under the New Investigator Program (NIP) in Earth Sciences, and the David and Lucile Packard Foundation and the Hewlett-Packard company through a Stanford University Terman Fellowship. I greatly

appreciate helpful comments and suggestions by Azadeh Tabazadeh, Andy Ackerman, Pat Hamill, Phil Russell, and Bob Bergstrom. I would also like to thank Patricia Quinn for supplying aerosol composition data over the ocean and Ann Fridlind for compiling statistics from the data set for use in Table 3.

References

Adams, P., J. H. Seinfeld, and D. M. Koch, Global concentrations of tropospheric sulfate, nitrate, and ammonium aerosol simulated in a general circulation model, *J. Geophys. Res., 104*, 13,791-13,823, 1999.

Andreae, M. O., Climatic effects of changing atmospheric aerosol levels, in *World Survey of Climatology*, vol. 16, *Future Climates of the World*, edited by A. Henderson-Sellers, pp. 341-392, Elsevier Sci., New York, 1995.

Andreae, M. O., et al., Airborne studies of aerosol emissions from savanna fires in southern Africa, 2, Aerosol chemical composition, *J. Geophys. Res., 103*, 32,119-32,128, 1998.

Arakawa, A., and V. R. Lamb, A potential enstrophy and energy conserving scheme for the shallow water equations, *Mon. Weather Rev., 109*, 18 - 36, 1981.

Bergstrom, R. W., Extinction and absorption coefficients of the atmospheric aerosol as a function of particle size, *Contrib. Atmos. Phys., 46*, 223-234, 1973.

Bergstrom, R. W., and P. B. Russell, Estimation of aerosol direct radiative effects over the mid-latitude North Atlantic from satellite and in situ measurements, *Geophys. Res. Lett., 26*, 1731-1734, 1999.

Berner, A., S. Sidla, Z. Galambos, C. Kruisz, R. Hitzenberger, H. M. ten Brink, and G. P. A. Kos, Modal character of atmospheric black carbon size distributions, *J. Geophys. Res., 101*, 19,559-19,565, 1996.

Bond, T. C., R. J. Charlson, and J. Heintzenberg, Quantifying the emission of light-absorbing particles: Measurements tailored to climate studies, *Geophys. Res. Lett., 25*, 337-340, 1998.

Boucher, O., and T. L. Anderson, General circulation model assessment of the sensitivity of direct climate forcing by anthropogenic sulfate aerosols to aerosol size and chemistry, *J. Geophys. Res., 100*, 26,117-26,134, 1995.

Charlson, R. J., J. Langner, H. Rodhe, C. B. Leovy, and S. G. Warren, Perturbation of the northern hemisphere radiative balance by backscattering from anthropogenic sulfate aerosols, *Tellus, 43AB*, 152-163, 1991.

Chin, M., D. J. Jacob, G. M. Gardner, M. S. Foreman-Fowler, and P. A. Spiro, A global three-dimensional model of tropospheric sulfate, *J. Geophys. Res., 101*, 18,667-18,690, 1996.

Chow, J. C., J. G. Watson, E. M. Fugita, Z. Lu, D. R. Lawson, and L. L. Ashbaugh, Temporal and spatial variations of PM2.5 and PM10 aerosol in the Southern California Air Quality Study, *Atmos. Environ., 28*, 2061-2080, 1994.

Chuang, C. C., J. E. Penner, K. E. Taylor, A. S. Grossman, and J. J. Walton, An assessment of the radiative effects of anthropogenic sulfate, *J. Geophys. Res., 102*, 3761-3778, 1997.

Cooke, W. F., and J. J. N. Wilson, A global black carbon aerosol model, *J. Geophys. Res., 101*, 19,395-19,409, 1996.

Cooke, W. F., C. Liousse, H. Cachier, and J. Feichter, Construction of a 1°x1° fossil fuel emission data set for carbonaceous aerosol and implementation and radiative impact in the ECHAM4 model, *J. Geophys. Res., 104*, 22,137-22,162, 1999.

Dentener, F. J., G. R. Carmichael, Y. Zhang, J. Lelieveld, and P. J. Crutzen, Role of mineral aerosol as a reactive surface in the global troposphere, *J. Geophys. Res., 101*, 22,869-22,889, 1996.

Deshler, T., D. J. Hofmann, B. J. Johnson, and W. R. Rozier, Balloonborne measurements of the Pinatubo aerosol size distribution and volatility at Laramie, Wyoming during the summer of 1991, *Geophys. Res. Lett., 19*, 199-202, 1992.

Ding, P., and D. A. Randall, A cumulus parameterization with multiple cloud-base levels. *J. Geophys. Res., 103*, 11,341-11,353, 1998.

Fang, M., M. Zheng, F. Wang, K. L. To, A. B. Jaafar, and S. L. Tong, The solvent-extractable organic compounds in the Indonesia biomass burning aerosols: - Characterization studies, *Atmos. Environ., 33*, 783-795, 1999.

Feichter, J., U. Lohmann, and I. Schult, The atmospheric sulfur cycle in ECHAM-4 and its impact on the shortwave radiation, *Clim. Dyn., 13*, 235-246, 1997.

Ferek, R. J., J. S. Reid, P. V. Hobbs, D. R. Blake, and C. Liousse, Emission factors of hydrocarbons, halocarbons, trace gases, and particles from biomass burning in Brazil, *J. Geophys. Res., 103*, 32,107-32,118, 1998.

Finlayson-Pitts, B. J., and J. N. Pitts Jr. *Atmospheric Chemistry: Fundamentals and Experimental Techniques*, John Wiley, New York, 1986.

Gillette, D. A., E. M. Patterson Jr., J. M. Prospero, and M. L. Jackson, Soil aerosols. in *Aerosol Effects on Climate*, edited by S. G. Jennings, pp. 73-109, Univ. of Ariz. Press, Tucson, 1993.

Gong, S. L., L. A. Barried, J. M. Prospero, D. L. Savoie, G. P. Ayers, J.-P. Blanchet, and L. Spacek, Modeling sea-salt aerosols in the atmosphere, 2, Atmospheric concentrations and fluxes, *J. Geophys. Res., 102*, 3819-3830, 1997.

Hack, J. J., J. T. Kiehl, and J. W. Hurrell, The hydrologic and thermodynamic characteristics of the NCAR CCM3, *J. Clim., 11*, 1179-1206, 1998.

Hänel, G., Radiation budget of the boundary layer, II, Simultaneous measurement of the mean solar volume absorption and extinction coefficients of particles, *Contrib. Atmos. Phys., 60*, 241-247, 1987.

Hansen, J., et al., Forcings and chaos in interannual to decadal climate change, *J. Geophys. Res., 102*, 25,679-25,720, 1997.

Hansen, J. E., M. Sato, A. Lacis, R. Ruedy, I. Tegen, and E. Matthews, Climate forcings in the industrial era, *Proc. Natl. Acad. Sci., U.S.A., 95*, 12,753-12,758, 1998.

Haywood, J. M., D. L. Roberts, A. Slingo, J. M. Edwards, and K. P. Shine, General circulation model calculations of the direct radiative forcing by anthropogenic sulfate and fossil-fuel soot aerosol, *J. Clim., 10*, 1562-1577, 1997.

Haywood, J. M. and V. Ramaswamy, Global sensitivity studies of the direct radiative forcing due to anthropogenic sulfate and black carbon aerosols, *J. Geophys. Res., 103*, 6043-6058, 1998.

Haywood, J. M., V. Ramaswamy, and B. J. Soden, Tropospheric aerosol climate forcing in clear-sky satellite observations over the oceans, *Science, 283*, 1299-1303, 1999.

Heintzenberg, J., R. J. Charlson, A. D. Clarke, C. Liousse, V. Ramaswamy, K. P. Shine, M. Wendisch, and G. Helas, Measurements and modelling of aerosol single-scattering albedo: Progress, problems and prospects, *Beitr. Phys. Atmos., 70*, 249-263, 1997.

Herman, J. R., N. Krotkov, E. Celarier, D. Larko, and G. Labow, Distribution of UV radiation at the Earth's surface from TOMS-measured UV-backscattered radiances, *J. Geophys. Res., 104*, 12,059-12,076, 1999.

Hignett, P., J. P. Taylor, P. N. Francis, and M. D. Glew, Comparison of observed and modeled direct aerosol forcing during TARFOX, *J. Geophys. Res., 104*, 2279-2287, 1999.

Hitzenberger, R., and H. Puxbaum, Comparisons of the measured and calculated specific absorption coefficients for urban aerosol samples in Vienna, *Aerosol Sci. Technol., 18*, 323-345, 1993.

Husar, R. B., J. M. Prospero, and L. L. Stowe, Characterization of tropospheric aerosols over the oceans with the NOAA advanced very high resolution radiometer optical thickness operational product, *J. Geophys. Res., 102*, 16,889-16,909, 1997.

Intergovernmental Panel on Climate Change (IPCC), Climate Change 1995, in *The Science of Climate Change*, edited by J. T. Houghton et al., Cambridge Univ. Press, New York, 572 pp., 1996.

Jacobson, M. Z., Global direct radiative forcing due to multicomponent anthropogenic and natural aerosols (abstract), *Eos Trans., AGU, 79*, F157, 1998.

Jacobson, M. Z., A study of the global direct radiative forcing due to multicomponent anthropogenic and natural aerosols, in *American Meteorological Society Symposium on Interdisciplinary Issues in Atmospheric Chemistry*, pp. 39-41, Am. Meteorol. Soc., Boston, Mass., 1999a.

Jacobson, M. Z., Isolating nitrated and aromatic aerosols and nitrated aromatic gases as sources of ultraviolet light absorption, *J. Geophys. Res., 104*, 3527-3542, 1999b.

Jacobson, M. Z., Studying the effects of calcium and magnesium on size-distributed nitrate and ammonium with EQUISOLV II, *Atmos. Environ., 33*, 3635-3649, 1999c.

Jacobson, M. Z., A physically-based treatment of elemental carbon optics: Implications for global direct forcing of aerosols, *Geophys. Res. Lett., 27*, 217-220, 2000.

Jayaraman, A., D. Lubin, S. Ramachandran, V. Ramanathan, E. Woodbridge, W. D. Collins, and K. S. Zalpuri, Direct observations of aerosol radiative forcing over the tropical Indian Ocean during the January-February 1996 pre-INDOEX cruise, *J. Geophys. Res. 103*, 13,827-13,836, 1998.

Kiehl, J. T., and B. P. Briegleb, The relative roles of sulfate aerosols and greenhouse gases in climate forcing, *Science, 260*, 311-314, 1993.

Kiehl, J. T., and K. E. Trenberth, Earth's annual global mean energy budget, *Bull. Am. Meteorol. Soc., 78*, 197-208, 1997.

Kiehl, J. T., J. J. Hack, G. B. Bonan, B. A. Boville, D. L. Williamson, and P. J. Rasch, The National Center for Atmospheric Research community climate model: CCM3, *J. Clim.*, *11*, 1131-1149, 1998.

Krekov, G. M., Models of atmospheric aerosols, in *Aerosol Effects on Climate*, edited by S. G. Jennings, pp. 9-72, Univ. of Ariz. Press, Tucson, 1993.

Krotkov, N. A., P. K. Bhartia, J. R. Herman, V. Fioletov, and J. Kerr, Satellite estimation of spectral surface UV irradiance in the presence of tropospheric aerosols, 1, Cloud-free case, *J. Geophys. Res.*, *103*, 8779-8793, 1998.

Langner, J., and H. Rodhe, A global three-dimensional model of the tropospheric sulfur cycle, *J. Atmos. Chem.*, *13*, 225-263, 1991.

Lelieveld, J., G.-J. Roelofs, L. Ganzeveld, J. Feichter, and H. Rodhe, Terrestrial sources and distribution of atmospheric sulphur, *Philos. Trans. R. Soc. London*, *352*, 149-158, 1997.

Li, S.-M., A. M. Macdonald, J. W. Strapp, Y.-N. Lee, and X.-L. Zhou, Chemical and physical characterizations of atmospheric aerosols over southern California, *J. Geophys. Res.*, *102*, 21,341-21,353, 1997.

Liao, H., and J. H. Seinfeld, Effect of clouds on direct aerosol radiative forcing and climate, *J. Geophys. Res.*, *103*, 3781-3788, 1998.

Li-Jones, X., H. B. Maring, and J. M. Prospero, Effect of relative humidity on light scattering by mineral dust aerosol as measured in the marine boundary layer, *J. Geophys. Res.*, *103*, 31,113-31,121, 1998.

Liousse, C., J. E. Penner, C. Chuang, J. J. Walton, H. Eddleman, and H. Cachier, A global three-dimensional model study of carbonaceous aerosols, *J. Geophys. Res.*, *101*, 19,411-19,432, 1996.

Miller, R. L., and I. Tegen, Climate response to soil dust aerosols, *J. Clim.*, *11*, 3247-3267, 1998.

Myhre, G., F. Stordal, K. Restad, and I. S. A. Isaksen, Estimation of the direct radiative forcing due to sulfate and soot aerosols, *Tellus*, *50B*, 463-477, 1998.

Mylonas, D. T., D. T. Allen, S. H. Ehrman, and S. E. Pratsinis, The source and size distributions of organonitrates in Los Angeles aerosol, *Atmos. Environ.*, *25A*, 2855-2681, 1991.

NASA Climate Data System Staff, Greenhouse effect detection experiment (GEDEX) selected data sets, NASA Goddard Space Flight Cent., Greenbelt, Md., 1992.

Nemesure, S., R. Wagener, and S. E. Schwartz, Direct shortwave forcing of climate by anthropogenic sulfate aerosol: Sensitivity to particle size, composition, and relative humidity, *J. Geophys. Res.*, *100*, 26,105-26,116, 1995.

O'Brien, R. J., J. H. Crabtree, J. R. Holmes, M. C. Hoggan, and A. H. Bockian, Formation of photochemical aerosol from hydrocarbons, *Environ. Sci. Technol.*, *9*, 577-582, 1975.

Penner, J. E., R. J. Charlson, J. M. Hales, N. S. Laulainen, R. Leifer, T. Novakov, J. Ogren, L. F. Radke, S. E. Schwartz, and L. Travis, Quantify and minimizing uncertainty of climate forcing by anthropogenic aerosols, *Bull. Am. Meteorol. Soc.*, *75*, 375-400, 1994.

Penner, J. E., C. C. Chuang, and K. Grant, Climate forcing by carbonaceous and sulfate aerosols, *Clim. Dyn.*, *14*, 839-851, 1998.

Pilinis, C., and X. Li, Particle shape and internal inhomogeneity effects on the optical properties of tropospheric aerosols of relevance to climate forcing, *J. Geophys. Res.*, *103*, 3789-3800, 1998.

Pilinis, C., S. N. Pandis, and J. H. Seinfeld, Sensitivity of direct climate forcing by atmospheric aerosols to aerosol size and composition, *J. Geophys. Res.*, *100*, 18,739-18,754, 1995.

Platt, C. M. R., A parameterization of the visible extinction coefficient of ice clouds in terms of the ice/water content, *J. Atmos. Sci.*, *54*, 2083-2098, 1997.

Pueschel, R., Atmospheric aerosols, in *Composition, Chemistry, and Climate of the Atmosphere*, edited by H. B. Singh, p. 145, Van Nostrand Reinhold, New York, 1995.

Quinn, P. K. and D. J. Coffman, Comment on "Contribution of different aerosol species to the global aerosol extinction optical thickness: Estimates from model results" by Tegen et al., *J. Geophys. Res.*, *104*, 4241-4248, 1999.

Quinn, P. K., D. J. Coffman, V. N. Kapustin, T. S. Bates, and D. S. Covert, Aerosol optical properties in the marine boundary layer during the First Aerosol Characterization Experiment (ACE 1) and the underlying chemical and physical aerosol properties, *J. Geophys. Res.*, *103*, 16,547-16,563, 1998.

Reid, J. S., P. V. Hobbs, R. J. Ferek, D. R. Blake, J. V. Martins, M. R. Dunlap, and C. Liousse, Physical, chemical, and optical properties of regional hazes dominated by smoke in Brazil, *J. Geophys. Res.*, *103*, 32,059-32,080, 1998.

Russell, P. B., P. V. Hobbs, and L. L. Stowe, Aerosol properties and radiative effects in the United States East Coast haze plume: An Overview of the Tropospheric Aerosol Radiative Forcing Observational Experiment (TARFOX), *J. Geophys. Res.*, *104*, 2213-2222, 1999a.

Russell, P. B., J. M. Livingston, P. Hignett, S. Kinne, J. Wong, A. Chien, R. Bergstrom, P. Durkee, and P. V. Hobbs, Aerosol-induced radiative flux changes off the United States mid-Atlantic coast: Comparison of values calculated from sunphotometer and in situ data with those measured by airborne pyranometer, *J. Geophys. Res.*, *104*, 2289-2307, 1999b.

Saxena, P., and L. M. Hildemann, Water-soluble organics in atmospheric particles: A critical review of the literature and application of thermodynamics to identify candidate compounds, *J. Atmos. Chem.*, *24*, 57-109, 1996.

Stelson, A. W., Urban aerosol refractive index prediction by partial molar refraction approach, *Environ. Sci. Technol.*, *24*, 1676-1679, 1990.

Stenchikov, G. L., I. Kirchner, A. Robock, H.-F. Graf, J. C. Antuna, R. G. Grainger, A. Lambert, and L. Thomason, Radiative forcing from the 1991 Mount Pinatubo volcanic eruption, *J. Geophys. Res.*, *103*, 13,837-13,857, 1998.

Sturges, W. T., and L. A. Barrie, Chlorine, bromine, and iodine in Arctic aerosols, *Atmos. Environ.*, *22*, 1179-1194, 1988.

Tabazadeh, A., M. Z. Jacobson, H. B. Singh, O. B. Toon, J. S. Lin, R. B. Chatfield, A. N. Thakur, R. W. Talbot, and J. E. Dibb, Nitric acid scavenging by mineral and biomass burning aerosols, *Geophys. Res. Lett.*, *25*, 4185-4188, 1998.

Talbot, R. W., J. E. Dibb, and M. B. Loomis, Influence of vertical transport on free tropospheric aerosols over central USA in springtime, *Geophys. Res. Lett.*, *25*, 1367-1370, 1998.

Tang, I., Thermodynamic and optical properties of mixed-salt aerosols of atmospheric importance, *J. Geophys. Res.*, *102*, 1883-1893, 1997.

Taylor, K. E., and J. E. Penner, Response of the climate system to atmospheric aerosols and greenhouse gases, *Nature*, *369*, 734-737, 1994.

Tegen, I., A. A. Lacis, and I. Fung, The influence on climate forcing of mineral aerosols from disturbed soils, *Nature*, 380, 419-422, 1996.

Tegen, I., P. Hollrig, M. Chin, I. Fung, D. Jacob, and J. Penner, Contribution of different aerosol species to the global aerosol extinction optical thickness: Estimates from model results. *J. Geophys. Res.*, *102*, 23,895-23,915, 1997.

Thomason, L. W., L. R. Poole, and T. Deshler, A global climatology of stratospheric aerosol surface area density deduced from Stratospheric Aerosol and Gas Experiment II measurements: 1984-1994, *J. Geophys. Res.*, *102*, 8967-8976, 1997.

Toon, O. B., and T. P. Ackerman, Algorithms for the calculation of scattering by stratified spheres, *Appl. Opt.*, *20*, 3657-3660, 1981.

Toon, O. B., C. P. McKay, T. P. Ackerman, and K. Santhanam, Rapid calculation of radiative heating rates and photodissociation rates in inhomogeneous multiple scattering atmospheres, *J. Geophys. Res.*, *94*, 16,287-16,301, 1989.

Venkataraman, C., J. M. Lyons, and S. K. Friedlander, Size distributions of polycyclic aromatic hydrocarbons and elemental carbon, 1, Sampling, measurement methods, and source characterization, *Environ. Sci. Technol.*, *28*, 555-562, 1994.

Wang, W.-C., M. P. Dudek, and X.-Z. Liang, The greenhouse effect of trace gases, in *World Survey of Climatology*, vol. 16, *Future Climates of the World*, edited by A. Henderson-Sellers, pp. 341-392, Elsevier Sci., New York, 1995.

Welch, R. M., S. K. Cox, and J. M. Davis, *Solar Radiation and Clouds*, *Meteorol. Monog. 17*, Am. Meteorol. Soc., Boston, Mass., 1980.

West, J. J., C. Pilinis, A. Nenes, and S. N. Pandis, Marginal direct climate forcing by atmospheric aerosols, *Atmos. Environ.*, *32*, 2531-2542, 1998.

Whitby, K. T., The physical characteristics of sulfur aerosols, *Atmos. Environ.*, 12, 135-159, 1978.

Xie, P., and P. A. Arkin, Analyses of global monthly precipitation using gauge observations, satellite estimates, and numerical model predictions, *J. Clim.*, *9*, 840-858, 1996.

M. Z. Jacobson, Department of Civil and Environmental Engineering, Terman Engineering Center, Room M-13, Stanford University, Stanford, CA 94305-4020. (e-mail: jacobson@ce.stanford.edu)

(Received April 7, 2000; revised July 14, 2000;
accepted August 28, 2000.)